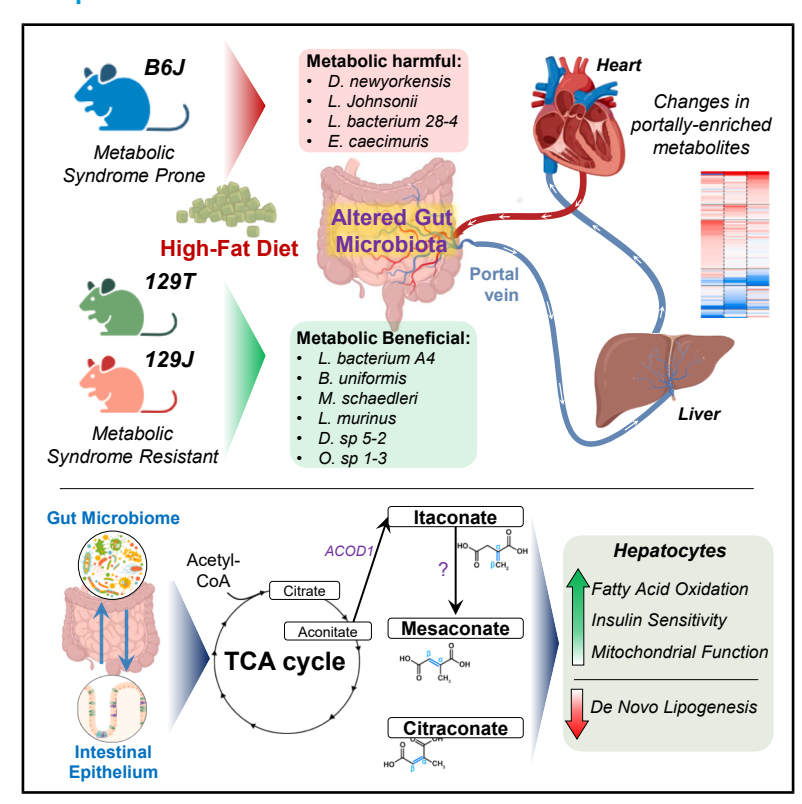
Portal vein-enriched metabolites as intermediate regulators of the gut microbiome in insulin resistance

Graphical abstract



Authors

Vitor Rosetto Muñoz, Francois Moreau, Marion Soto, ..., Aleksandar Kostic, Clary B. Clish, C. Ronald Kahn

Correspondence

c.ronald.kahn@joslin.harvard.edu

In brief

Muñoz et al. show that circulating metabolites are differentially enriched in portal versus peripheral blood. Enrichment patterns are influenced by diet, host genetics, and the gut microbiome. These metabolites, especially mesaconate/itaconate/citraconate isomers, can directly influence hepatic insulin signaling and gene expression, highlighting an important role in obesity-linked insulin resistance.

Highlights

- Portal and peripheral blood show distinct metabolite profiles across strains and diets
- Portal metabolite enrichment is shaped by diet, microbiota, and host genetics
- Antibiotics modulate portal metabolites, including TCArelated mesaconate isomers
- Mesaconate isomers regulate insulin signaling, gene expression, and liver fat levels









Article

Portal vein-enriched metabolites as intermediate regulators of the gut microbiome in insulin resistance

Vitor Rosetto Muñoz,^{1,7} Francois Moreau,^{1,7} Marion Soto,¹ Yoshiyuki Watanabe,¹ Loc-Duyen Pham,⁴ Jimmy Zhong,⁴ Sam Zimmerman,⁴ Bruna B. Brandao,¹ Khyati Girdhar,⁶ Julian Avila,² Hui Pan,³ Jonathan M. Dreyfuss,³ Michael Y. Mi,⁵ Robert E. Gerszten,⁵ Emrah Altindis,⁶ Aleksandar Kostic,⁴ Clary B. Clish,² and C. Ronald Kahn^{1,8,*}

SUMMARY

Diet and obesity contribute to insulin resistance and type 2 diabetes, in part via the gut microbiome. To explore the role of gut-derived metabolites in this process, we assessed portal/peripheral blood metabolites in mice with different risks of obesity/diabetes, challenged with a high-fat diet (HFD) + antibiotics. In diabetes/ obesity-prone C57BL/6J mice, 111 metabolites were portally enriched and 74 were peripherally enriched, many of which differed in metabolic-syndrome-resistant 129S1/129S6 mice. Vancomycin treatment of HFD-fed C57BL/6J mice modified the microbiome and the portal/peripheral ratio of many metabolites, including upregulating tricarboxylic acid (TCA) cycle-related metabolites, like mesaconate, in portal blood. Treatment of isolated hepatocytes with mesaconate, itaconate, or citraconate improved insulin signaling and transcriptionally regulated genes involved in gluconeogenesis, fatty acid oxidation, and lipogenesis *in vitro* and *in vivo*. In humans, citraconate levels are inversely correlated with plasma glucose. Thus, portal versus peripheral metabolites play important roles in mediating effects of the microbiome on hepatic metabolism and the pathogenesis of HFD-related insulin resistance.

INTRODUCTION

Insulin resistance is central to type 2 diabetes (T2D), obesity, and the metabolic syndrome, all of which are products of gene-environment interactions. A major mediator of gene-environment interactions is the gut microbiome. Multiple studies have identified significant differences in gut microbiota in humans and rodents with obesity/T2D. ^{1,2} In general, elevated abundance of Firmicutes compared with Bacteroidetes and Proteobacteria is associated with insulin resistance, obesity, and glucose intolerance. ^{1,3,4} Individuals with T2D also tend to have lower levels of potentially beneficial butyrate-producing species, such as *Eubacterium rectale*, *Faecali prausnitzii*, and *Roseburia*, ⁵ as well as *Akkermansia*, which have been linked to improved metabolic profiles through anti-inflammatory effects. ⁶ These findings are supported by studies transferring microbiota from obese or diabetic donors into germ-free mice. ^{2,7–9}

The gut microbiome impacts systemic metabolism through multiple mechanisms. It modulates intestinal permeability/

motility^{10,11} and gut hormone secretion¹² and produces metabolites that affect host physiology, ^{13,14} including bile acids, ^{15,16} short-chain fatty acids (SCFAs), ^{17–21} branched-chain amino acids (BCAAs), ²² and trimethylamine (TMA). ²³ Although a few studies have assessed portal blood metabolites in specific contexts, ^{24–26} most metabolomic studies assess peripheral blood, potentially underestimating the effects of gut microbial metabolites, which pass through the portal vein to the liver, ²⁷ where they may be cleared or modified before reaching the systemic circulation (Figure S1A).

In this study, we have characterized the effect of gut microbiota and their changes in response to high-fat diet (HFD) and antibiotics (vancomycin and metronidazole) on the levels of metabolites in both the portal and peripheral/cardiac circulation, as well as the nature of portal/peripheral metabolites in mice with differing propensity to metabolic syndrome on HFD. In line with previous work, ^{9,28,29} gut microbiota exhibit major changes with the introduction of an HFD diet/antibiotics and among strains of mice. Consistent with our hypothesis, we find that



Section of Integrative Physiology and Metabolism, Joslin Diabetes Center, Harvard Medical School, Boston, MA, USA

²Metabolomics Platform, Broad Institute of MIT and Harvard University, Cambridge, MA, USA

³Bioinformatics and Biostatistics Core, Joslin Diabetes Center, Harvard Medical School, Boston, MA, USA

⁴Section on Pathophysiology and Molecular Pharmacology, Joslin Diabetes Center, Harvard Medical School, Boston, MA, USA

⁵Division of Cardiovascular Medicine, Beth Israel Deaconess Medical Center, Harvard Medical School, Boston, MA, USA

⁶Biology Department Boston College, Chestnut Hill, MA, USA

⁷These authors contributed equally

⁸Lead contact

^{*}Correspondence: c.ronald.kahn@joslin.harvard.edu https://doi.org/10.1016/j.cmet.2025.08.005



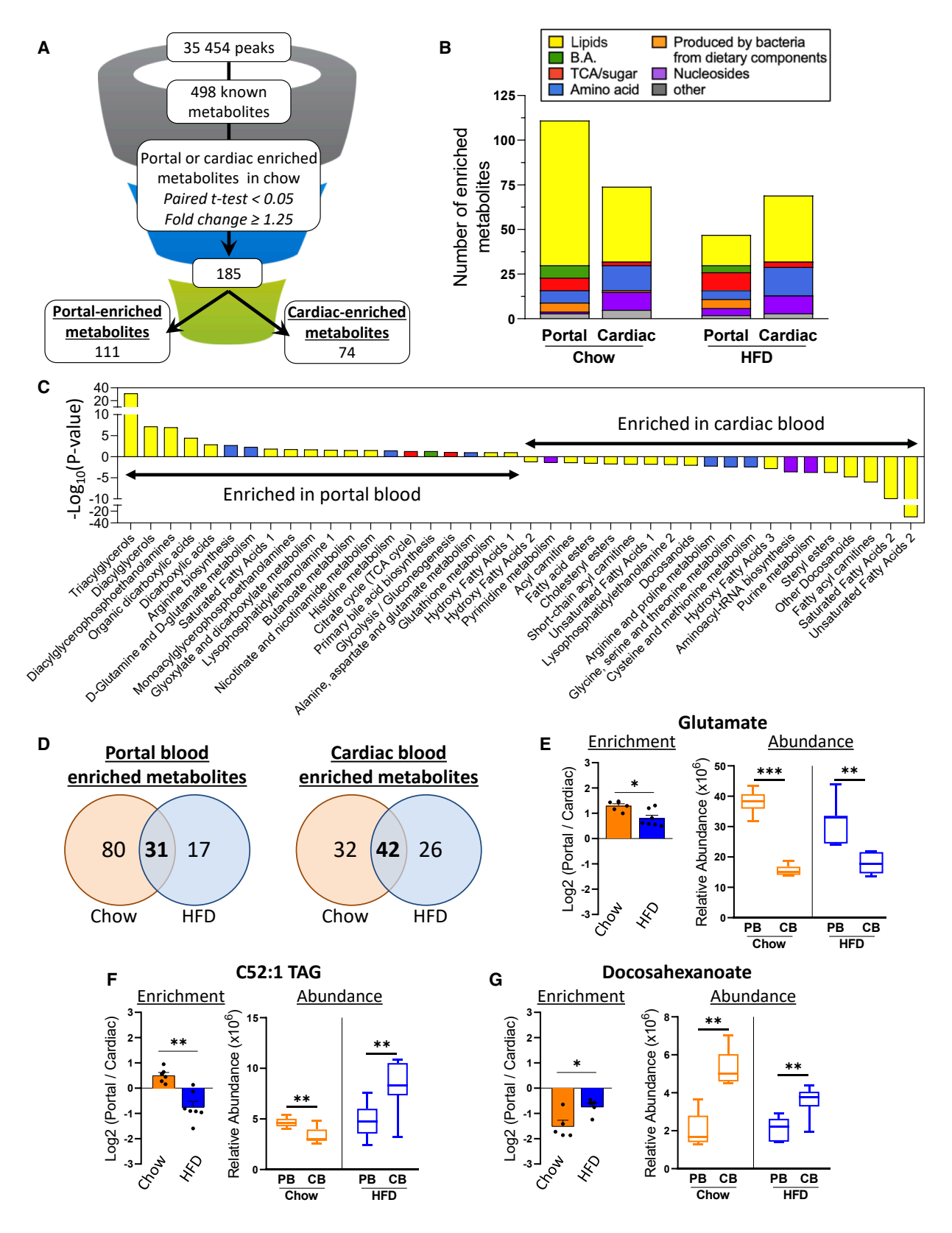


Figure 1. Portal blood metabolites exhibit a unique signature in response to HFD

(A) Workflow of identification of portal- and cardiac-enriched metabolites (p < 0.05 and fold change > 1.25).

(B) Bar graph representation of the different classes of metabolites enriched in the portal and cardiac/systemic blood in C57BL/6J mice on chow and HFD.



Cell MetabolismArticle

peripheral and portal blood have unique metabolomic profiles, many of which can be linked to differences in the microbiome. Among the portally enriched metabolites, several tricarboxylic acid (TCA) cycle-related intermediates (aconitate, mesaconate, citrate, and 2-hydroxyglutarate) could be linked to changes in the gut microbiome at a metagenomic level. Importantly, in vitro treatment of hepatocytes with mesaconate, itaconate, and citraconate increased insulin-stimulated AKT phosphorylation and increased expression of genes involved in fatty acid oxidation, as well as mitochondrial oxidative activity, while downregulating genes involved in de novo lipogenesis. These effects were also observed in vivo and are consistent with findings in human epidemiological studies. These data demonstrate the importance of microbiome/intestine-derived metabolites, especially the TCA cycle intermediate mesaconate and related molecules, on insulin sensitivity and the importance of understanding portal versus peripheral differences in defining their implications for host metabolism and health.

RESULTS

Portal and peripheral blood have different metabolomic profiles

We and others have shown that gut microbiota play a major role in the phenotype of diabetes/obesity-prone C57BL/6J (B6J) mice. 9,28,29 Thus, HFD-fed B6J mice exhibit weight gain, decreased insulin sensitivity, and glucose intolerance. These phenotypes are improved by antibiotic treatment, which alters the gut microbiome, and can be reproduced by the transfer of gut bacteria of these mice into germ-free animals.²⁹ To determine the role of circulating metabolites in this process, portal and cardiac blood were collected from these mice under four conditions (chow diet, HFD, HFD + vancomycin, or HFD + metronidazole) and assessed by liquid chromatography-mass spectrometry (LC-MS). 9,28 The abundances of ~35,450 peaks were measured, 498 of which were identified using reference standards (Figure 1A). Consistent with other studies,²⁴ principalcomponent analysis (PCA) analysis of metabolites from these mice revealed two distinct groups representing portal and cardiac blood (Figure S1B). Indeed, metabolite clustering was more dependent on the vascular site of sampling than on diet or antibiotic treatment.

In chow-fed animals, 111 metabolites were significantly enriched in portal blood and 74 enriched in cardiac blood, defined as a >11.25l-fold-difference and p < 0.05 (Figure 1A). Among portally enriched metabolites, 73% were lipids, including various triglycerides, diacylglycerols, and phospholipids (Figures 1B, 1C, and S1C). Another 6% of portal-enriched metabolites were primary or secondary bile acids, while 7 were amino acids/Nacetyl-amino acids (6%), and 4.5% were bacterial metabolites derived from food, such as butyrate, tryptophan, histidine, and vitamin A-derived metabolites (Figures 1B, 1C, and S1C). Sur-

prisingly, several portally enriched metabolites were related to the TCA cycle (aconitate, mesaconate, and 2-hydroxyglutarate) or gluconeogenesis (phosphoglycerate/phosphoinositolpyruvate) (Figures 1B, 1C, and S1C). The higher concentration of these metabolites in portal versus cardiac blood suggests that the gut microbiome, food, and/or the intestine are major contributors of these metabolites to the circulation. By contrast, 74 metabolites were significantly enriched in cardiac (peripheral) blood. 57% of these were lipids, including other species of triglycerides, diacylglycerides, phospholipids, cholesteryl esters, docosanoids, and eicosanoids; 19% were amino acids (methionine, histidine, tryptophan, and lysine); and 13.5% were nucleosides or their derivatives, including AMP, UMP, guanosine monophosphate (GMP), inosine, and hypoxanthine, all of which showed 2.7- to 3.4-fold enrichment in cardiac blood (Figures 1B, 1C, and S1C). The high cardiac/portal ratio suggests that these metabolites are, at least in part, contributed by the liver or other host tissues.

Portal metabolite enrichment—Effects of diet

The composition of metabolites in portal/cardiac blood in mice changed significantly in mice on 60% HFD for 11 weeks. The number of metabolites enriched in portal blood decreased from 111 to 48 (with 31 the same as on chow), while cardiac blood-enriched metabolites decreased from 74 on normal chow to 68 on HFD, with 42 unaffected (Figures 1B and 1D). Reduction in portally enriched metabolites was primarily due to a decrease in portally enriched lipids, which dropped from 81 to 17 species in HFD-fed mice (Figures 1B, 1D, and S1D). The 31 portally enriched metabolites unchanged between chow and HFD included multiple TCA cycle-related metabolites, suggesting they were derived from either the microbiome or intestine rather than the diet. Conversely, 40 species, mainly lipids, demonstrated significant changes in enrichment with changing diet (Figure S1D). Most of these (26/40) lost portal enrichment on HFD, while only C36:5 PC plasmalogen-A gained portal enrichment (Figure S1D). Aspartate, glutamate, C56:10 TAG, and C36:3 PE were changed by HFD but remained enriched in portal blood (Figure 1E). Nine portally enriched TAGs shifted enrichment from portal to cardiac blood in HFD mice, suggesting that the portal-peripheral difference reflects either hepatic contributions to these lipids, differences in intestinal TAG/DAG secretion, or differences in lymphatic and venous absorption of different lipid species (Figures 1F, S1D, and S1G).

While the number of metabolites enriched in cardiac blood was similar on chow and HFD feeding, 6 cardiac-enriched metabolites had reduced enrichment on HFD, including docosahexanoate, eicosapentaenoic acid, and 20-HDoHE—all omega-3 fatty acids or derivatives with anti-inflammatory properties (Figures 1G and S1D–S1l). By contrast, proinflammatory omega-6-derived fatty acids, including eicosadienoic acid, γ -linoleic acid, arachidonate, and adrenate, increased in abundance in response to HFD in both

⁽C) Pathways represented by the metabolites enriched in portal and cardiac blood.

⁽D) Venn diagram indicating the number of portal (top) or cardiac (bottom) enriched metabolites in mice on chow or HFD (paired t test p < 0.05 and fold change > 1.25).

⁽E–G) Histogram illustrating metabolite enrichment measured as \log_2 of the ratio of portal abundance/cardiac abundance (left) and boxplot (right) of the relative abundance for glutamate (E), C52:1 DAG (F), and docosahexanoate (G). Data are expressed as mean \pm SEM (chow [n = 6] and HFD [n = 7]; *p < 0.05, **p < 0.01, ***p < 0.001; unpaired t test for the enrichment and paired t test for the abundance).

Article



circulations (Figures S1D–S1I). These increased proinflammatory and reduced anti-inflammatory metabolites likely contribute to the increased insulin resistance associated with HFD. 30,31

Gut microbiome profile and TCA cycle metabolite enrichment in portal blood

To assess the impact of the microbiome, two groups of HFD-fed mice were given antibiotics-either vancomycin, which targets gram+ organisms, or metronidazole, targeting gram- and gram-+ anaerobes. 32 As previously shown, in obesity/diabetes-prone HFD-fed B6J mice, both antibiotics produced major changes in gut microbiota and improved insulin resistance and glucose tolerance.²⁸ The changes in metabolites with HFD and antibiotics were associated with dramatic alterations of gut microbiota (Figure 2A), with HFD inducing decreases of Lactobacillus, Bacteroides, and Parabacteroides and increases in Staphylococcus and Lachnospiraceae (Figure 2B). Treatment with both antibiotics led to a loss of Lachnospiraceae and Helicobacter (Figure 2B). In the vancomycin-treated group, this was associated with increases in Proteus, Bacillus, Enterococcus, Lactobacillus, and Clostridium species, whereas metronidazole treatment led to increases of Proteus and Paenibacillus species (Figure 2B). Compared with chow, Shannon diversity and Bray-Curtis indices were lower in mice on HFD, and this was somewhat reversed by metronidazole treatment (Figures S2A and S2B). These changes were paralleled by changes at the species level (Figure S2C).

In the portal circulation, both antibiotics induced significant changes in the abundance of multiple metabolites, with \sim 1.5fold increases of 2-hydroxglutarate and mesaconate (metabolites related to the TCA cycle) and a 1.2-fold increase in citrulline (Figures 2C, S3A, and S3B). As expected, antibiotic treatment led to 4- to 5-fold increases in portal levels of two primary bile acids, tauro-muricholic acid and taurocholic acid, as well as reduction of portal levels of secondary and primary unconjugated bile acids produced by gut bacteria (deoxycholate, hyodeoxycholic acid, tauro-lithocholic acid, and chenodeoxycholate A) (Figures 2C and S2D). These changes in bile acids are likely due to impaired microbial metabolism and subsequent reabsorption into the portal circulation and hepatic reuptake. Two metabolites (ketodeoxycholate and aconitate) were increased in portal concentration by metronidazole (Figure 2C), whereas nine exhibited increases in enrichment in cardiac blood following vancomycin treatment (putrescine, 4-pyridoxate, 6,8-dihydroxypurine, and six triglyceride species) (Figure 2C).

As a result, portal versus cardiac enrichment was altered for multiple metabolites by antibiotic treatment. Thus, both azelate and sebacate were enriched in portal blood of mice on chow and HFD but showed decreased enrichment with metronidazole treatment (Figures 2D and S2E). Conversely, vancomycin increased proline enrichment in portal blood (Figures S3A and S3B). Likewise, hydroxyproline and ornithine showed increased enrichment in portal blood in HFD mice following antibiotic treatment (Figures S3A and S3B), while arginine (Figures S3A and S3B), another urea cycle metabolite, was enriched in cardiac blood independent of diet or antibiotics (Figures S3A and S3B). In some cases, antibiotic treatment created a portal/peripheral gradient for a metabolite not observed by HFD alone. Thus, uridine and uracil did not exhibit enrichment in either portal or car-

diac blood in mice on chow or HFD, but treatment of HFD mice with vancomycin, and to a lesser extent metronidazole, resulted in significant enrichment of these metabolites in cardiac blood (Figures 2E, S2F, and S3C). Metabolites related to histidine and purine metabolism, which were also cardiac enriched, were unchanged by antibiotic treatment (Figures S3D and S3E). In addition, plasma levels of DAG C36:1, DAG, and C54:2 and C51:1 TAGs showed increased cardiac enrichment by vancomycin (Figure S3F).

TCA cycle metabolite enrichment in portal blood

The changes in microbiota following antibiotics were mirrored by changes in TCA cycle-related metabolites. Thus, citrate/isocitrate, aconitate, mesaconate, and 2-hydroxyglutarate showed portal enrichment in chow- and HFD-fed B6J mice, which further increased with vancomycin and, to a lesser extent, metronidazole (Figure 3A). Metagenomic data revealed positive correlations of these changes with the relative abundances of Akkermansia, Proteus sp., Gammaproteobacteria, Enterobacterales, Lactococcus, and Lactobacillales (Figure 3B). Importantly, metagenomic data on the microbial genes encoding TCA cycle enzymes required for production of these metabolites also increased in the vancomycin-treated HFD group, indicating that these metabolites are likely derived from gut microbiota (Figure 3C). Expression of several TCA cycle enzymes (Pdha, Cs, Aco1, Acod1, Sdhb, and Mdh2) and the itaconate-mesaconate converting enzyme (Suclg1) was upregulated in colonic epithelium by vancomycin treatment (Figures 3D and S3G), suggesting a possible contribution from the intestine as well.

Integrating microbiome differences and antibiotic effects with strain differences

We have previously shown that B6J mice develop obesity/insulin resistance when fed HFD, whereas 129S1 mice from Jackson Labs (129J) and 129S6 (129T) mice from Taconic are metabolic syndrome resistant²⁸ (Figure 4A). Thus, following 12 weeks of HFD, weights of B6J mice were higher than those of both 129 strains (Figure 4B), as was the level of insulin resistance/ HOMA-IR (22.7 \pm 2.9 versus 5.6 \pm 0.8 and 5.8 \pm 0.6) (Figure 4C). Hepatic gene expression was consistent with these metabolic differences, with lower levels of the lipogenic transcription factor Srebp1c and Srebp1c target genes Acc, Fas, and Scd1 in the liver of both 129 strains but no differences in expression of gluconeogenic genes (G6pc, Pck1, and Fbp1) (Figure 4D). Likewise, expression of Igfbp2, which inversely correlates with hepatic steatosis and insulin resistance, 33 was increased by 4-fold in both strains of 129 mice as compared with B6J.

To determine how gut microbial metagenomes contribute to the gene expression differences between strains, we compared the microbiomes in HFD-fed B6J, 129J, and 129T mice (Figure 4E) to identify bacteria that could be metabolically beneficial (class I) or metabolically harmful (class II) based on their abundance in different strains. Class I, potentially beneficial, microbes were exemplified by *L. bacterium A4* (higher in 129J/129T versus B6J); *B. uniformis*, *P. goldsteinii*, *B. massiliensis*, *M. schaedleri*, and *L. murinus* (higher in 129T mice versus B6J); and *D. sp 5-2*, *E. faecalis*, *A. celatus*, *A. equolifaciens*, *L. bacterium M18-1*, *O. sp 1-3*, *L. lactis*, and *C. cocleatum* (higher



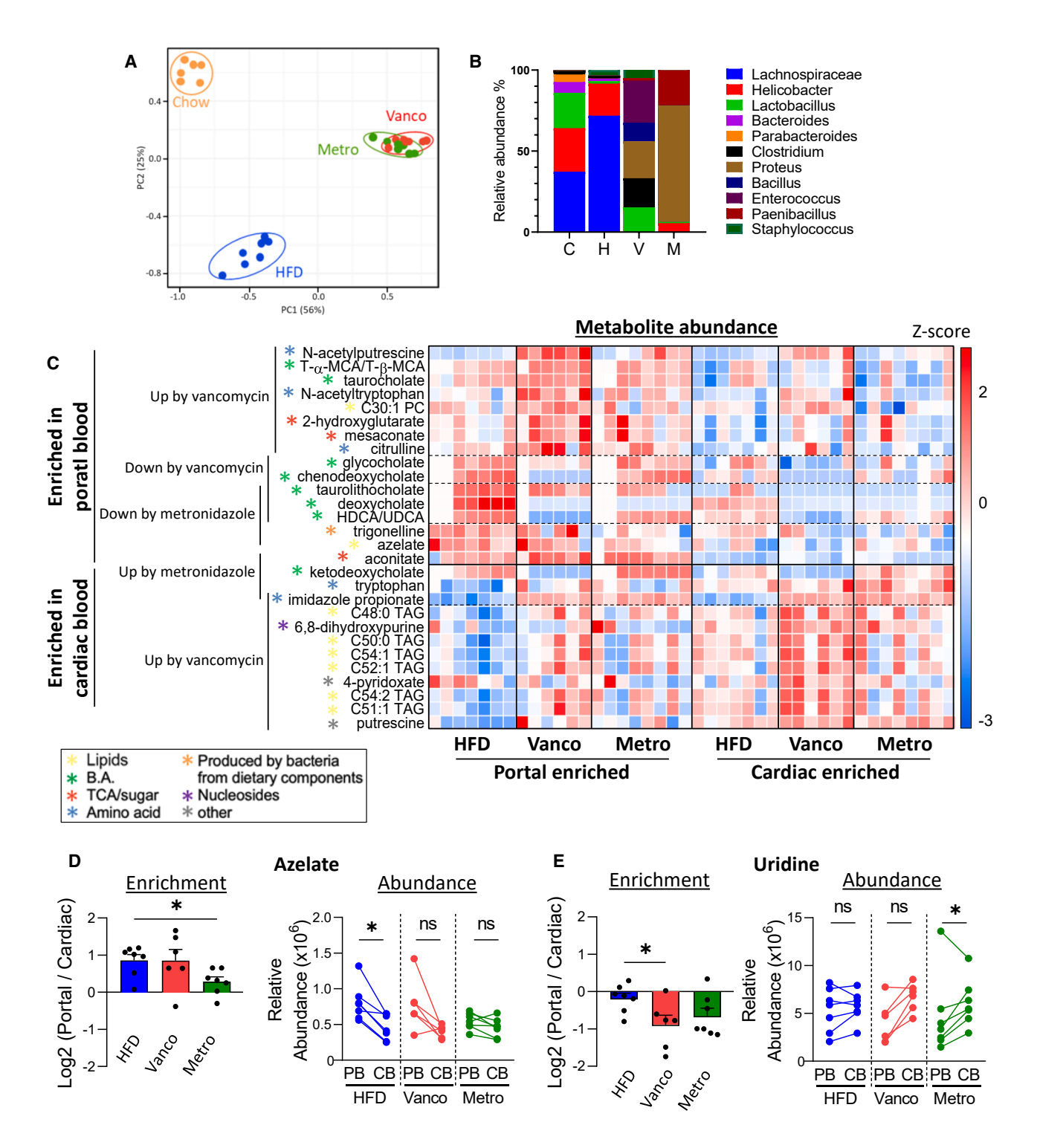


Figure 2. Treatment of HFD mice with antibiotics increases TCA/urea cycle-related metabolites in portal blood
(A) Principal-component analysis (PCA) plot of gut bacteria in cecal samples from mice on chow, HFD, HFD + vancomycin, and HFD + metronidazole.
(B) Graphical representation of the gut bacteria genera in the cecum of mice on chow "C," HFD "H," HFD + vancomycin "V," and HFD + metronidazole "M."
(C) Heatmaps representing portal and cardiac blood-enriched metabolites showing significant changes (unpaired t test p < 0.05) induced by vancomycin or metronidazole treatment of HFD mice. Histogram illustrating the enrichment (left) and graphical representation of individual values of the relative abundance (right) for azelate (D) and uridine (E). Data are expressed as mean \pm SEM for enrichment and as individual values for the abundance (n = 6-7; ns, non-significant; p < 0.05, unpaired t test for the enrichment and paired t test for the abundance).



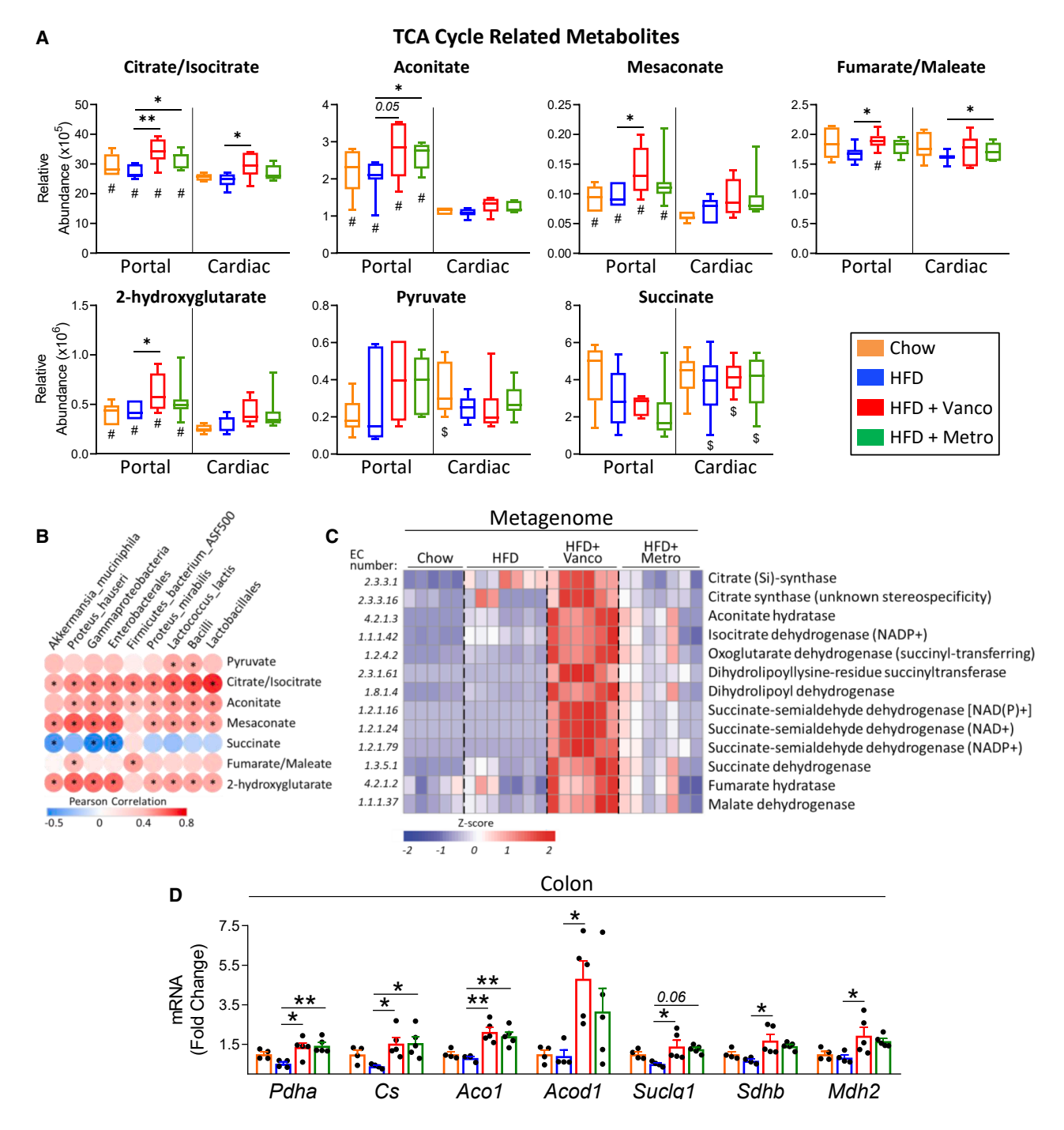


Figure 3. Reshaping gut microbiota leads to portal enrichment of TCA cycle metabolites

(A) Boxplots of the relative abundance of metabolites from the TCA cycle in portal and cardiac blood from mice on chow (n = 6), HFD (n = 7), HFD + vancomycin (Vanco) (n = 6), and HFD + metronidazole (Metro) (n = 7-8). *p < 0.05, **p < 0.05,

(B) Heatmap showing the correlation coefficients of portal blood TCA cycle metabolites and gut bacteria species (Pearson correlation *p < 0.05).

(C) Heatmap demonstrating the contribution of the gut microbiome to the main enzymatic reactions of the TCA cycle based on the Enzyme Commission (EC) numbers and the metagenomic data.

(D) Gene expression of TCA cycle enzymes (Pdha, Cs, Aco1, Acod1, Suclg1, Sdhb, and Mdh2) in the colon of B6J mice under chow, HFD, HFD + vancomycin (Vanco), and HFD + metronidazole (Metro) (n = 4–5). Gene expression was normalized to the level of 36b4. Data are expressed as mean \pm SEM (*p < 0.05, **p < 0.01; one-way ANOVA followed by Tukey's post test; #, portal-enriched; \$, cardiac enriched).



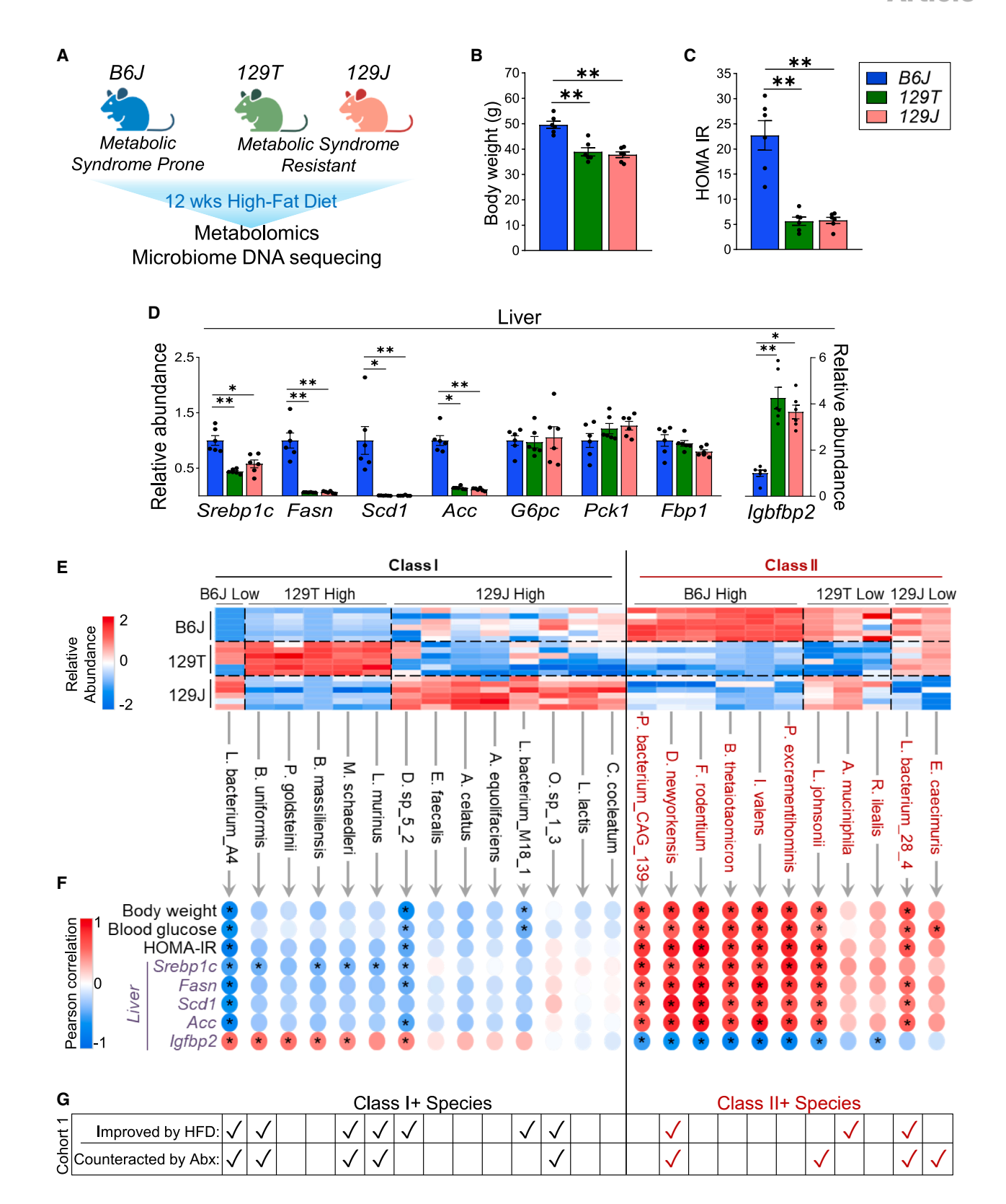


Figure 4. C57BL/6J mice are prone to develop obesity and insulin resistance as compared with 129S6/SvEvTac (129T) and 129S1/SvImJ (129J) mice

(A) Schematic representation of the three strains (B6J, 129T, and 129J) used in the experiment. 8-week-old animals were on HFD for 12 weeks, after which samples were collected for metabolomics and microbiota profiling.

Article



in 129J versus B6J) (Figure 4E). Indeed, class I bacteria showed significant negative correlations with body weight, blood glucose, HOMA-IR, and hepatic lipogenic markers and positive correlations with hepatic lgfbp2, consistent with a role in insulin sensitivity and reduced body weight (Figure 4F). Class II, potentially harmful, microbes, on the other hand, included P. bacterium CAG 139, D. newyorkensis, F. rodenttium, B. thetaiotaomicron, I. valens, and P. excrementihominis (lower in abundance in 129J/129T compared with B6J); L. johnsonii, A. muciniphila, and R. ilealis (lower in 129T versus B6J); and L. bacterium 28-4 and E. caecimuris (lower in 129J versus B6J) (Figure 4E). Class II microbes showed positive correlations with body weight, blood glucose, HOMA-IR, and hepatic lipogenic enzyme expression, and a negative correlation with hepatic Igfbp2 (Figure 4F), consistent with a role of these in insulin resistance and metabolic syndrome.

These strain-specific differences in microbiota in cohort 2 could be further refined as potentially beneficial versus harmful based on their response to HFD and antibiotics in B6J mice in cohort 1 (Figure 4G). Of the 14 potentially beneficial microbiota identified in the strain comparison, 6 were lower in B6J mice on HFD compared with chow (L. bacterium A4, B. uniformis, M. schaedleri, L. murinus, O. sp 1-3, and D. sp 5-2), and 5 of these were rescued by antibiotic treatment (Figures 4G and S4A). We termed these class I+, indicating they were associated with insulin sensitivity in the comparison of mouse strains and in the analysis of the effects of HFD/antibiotics in B6J mice. Conversely, 11 class II microbial species were enriched in HFD-fed B6J mice relative to the 129 strains and thus potentially harmful. Two (D. newyorkensis and L. bacterium 28-4) were upregulated by HFD and attenuated by antibiotics in cohort 1, and another two (L. johnsonii and E. caecimuris) were attenuated by antibiotics (Figures 4G and S4B), consistent with a role as drivers of metabolic syndrome. We termed these class II+ microbes.

Using metagenomic data from the microbial analysis, we sought to identify specific metabolic pathways enriched in class I+ versus class II+ bacteria linked to beneficial or adverse effects. Indeed, *L. bacterium A4* and *D. sp 5-2*, which were more abundant in 129J versus B6J, attenuated by HFD, and recovered by antibiotics in B6J (class I+), showed reduced presence of microbial genes in pathways related to galactose degradation, ketogenesis, L-phenylalanine degradation, and peptidoglycan biosynthesis and positive association with genes linked to L-lysine biosynthesis, L-tryptophan biosynthesis, gluconeogenesis, and glycolysis (Figure S4C). By contrast, *D. newyorkensis* and *L. bacterium 28-4*, which were enriched in the B6J versus 129 microbiota, increased by HFD and attenuated by antibiotics, i.e., class II+ microbes, showed a negative association of microbial genes related to L-tryptophan biosynthesis, gluconeogen-

esis, L-isoleucine biosynthesis, and glycolysis, but a positive association with genes involved in ketogenesis, L-phenylalanine degradation, L-glutamine biosynthesis, and galactose degradation (Figure S4C).

Class I+ and II+ bacteria were associated with strainspecific portal/cardiac enrichment

To integrate host effects, gut microbial profile, and portal enrichment of metabolites, we performed metabolomics in portal/cardiac blood of B6J, 129J, and 129T mice on HFD. Interestingly, only 27 metabolites were portally enriched in all three strains, while 28 were exclusively enriched in B6J mice, 12 exclusively enriched in 129T mice, and 41 exclusively enriched in 129J mice (Figures S5A and S5B). Likewise, 14 metabolites were cardiac-blood-enriched exclusively in B6J, 19 in 129T, and 7 in 129J, with 24 metabolites cardiac enriched in all strains (Figures S5A and S5C). Strain-specific enrichment included stearate, which was portally enriched in B6J but not in 129T/ 129J mice (Figure S5D), whereas acetyl-galactosamine was portally enriched in 129T/129J strains but not in B6J mice (Figure S5E). Cardiac-enriched metabolites also exhibited strain-specific differences. C4 carnitine was \sim 2-fold cardiac enriched in B6J but not enriched in either the 129 strain (Figure S5F). Methionine sulfoxide, on the other hand, was enriched ~4-fold in cardiac blood of 129T and 129J mice, but not in the B6J (Figure S5G). Similarly, C2 carnitine showed portal enrichment in 129T/129J but cardiac enrichment in B6J mice, while glycerate showed portal enrichment in B6J but no enrichment in 129T/129J mice. Some metabolites like acetyltyrosine and acisoga were portally enriched across all strains but with quantitative differences between strains (Figures 5A and S5H). These strain-specific differences in portal/cardiac blood metabolites could contribute to the differences in metabolic syndrome risk among strains.

The changes in portal metabolite concentration were not well correlated with cecal metabolomics. Indeed, of the 243 metabolites identified in both the cecal content and portal blood, only 32 (13.2%) positively correlated (p < 0.05) between these sites. This is not surprising, since metabolites can be generated and absorbed in different regions of the gut and appear enriched in portal blood. Moreover, it is possible that the gut microbiome communicates with intestinal cells and surrounding cells to produce or utilize metabolites, and this could add to differences between the cecum and portal blood concentrations. Thus, while some metabolites like glycerate, acisoga, p-hydroxyphenylacetate, and adipate/methylglutarete showed significant correlation with the cecal abundance, many others did not (Figure S5I).

To further explore the relationship between metabolically beneficial (class I+) and metabolically harmful (class II+) bacteria,

⁽B and C) (B) Body weight and (C) HOMA-IR in C57BL/6J (n = 6), 129T (n = 6), and 129J (n = 6).

⁽D) Expression of genes of lipogenesis (Srebp1c, Fas, Scd1, and Acc), gluconeogenesis (G6pc, Pck1, and Fbp1), and an insulin sensitivity marker (Igfbp2) in the liver, all normalized to the level of 36b4. Data are expressed as mean \pm SEM and further normalized to the level in C57BL/6J mice (n = 6) (*p < 0.05, **p < 0.01; Kruskal-Wallis followed by a Dunn's multiple comparison).

⁽E) Heatmap illustrating the variation of abundance of gut bacterial species (class I and class II) in B6J, 129T, and 129J. Data are expressed as relative abundance (n = 6)

⁽F) Heatmap illustrating the Pearson correlation of species-specific bacteria in the gut with physiological parameters (body weight, blood glucose, and HOMA-IR) and hepatic genes (Pearson correlation *p < 0.05).

⁽G) Box showing the bacteria species that were improved by HFD or counteracted by antibiotics in cohort 1.



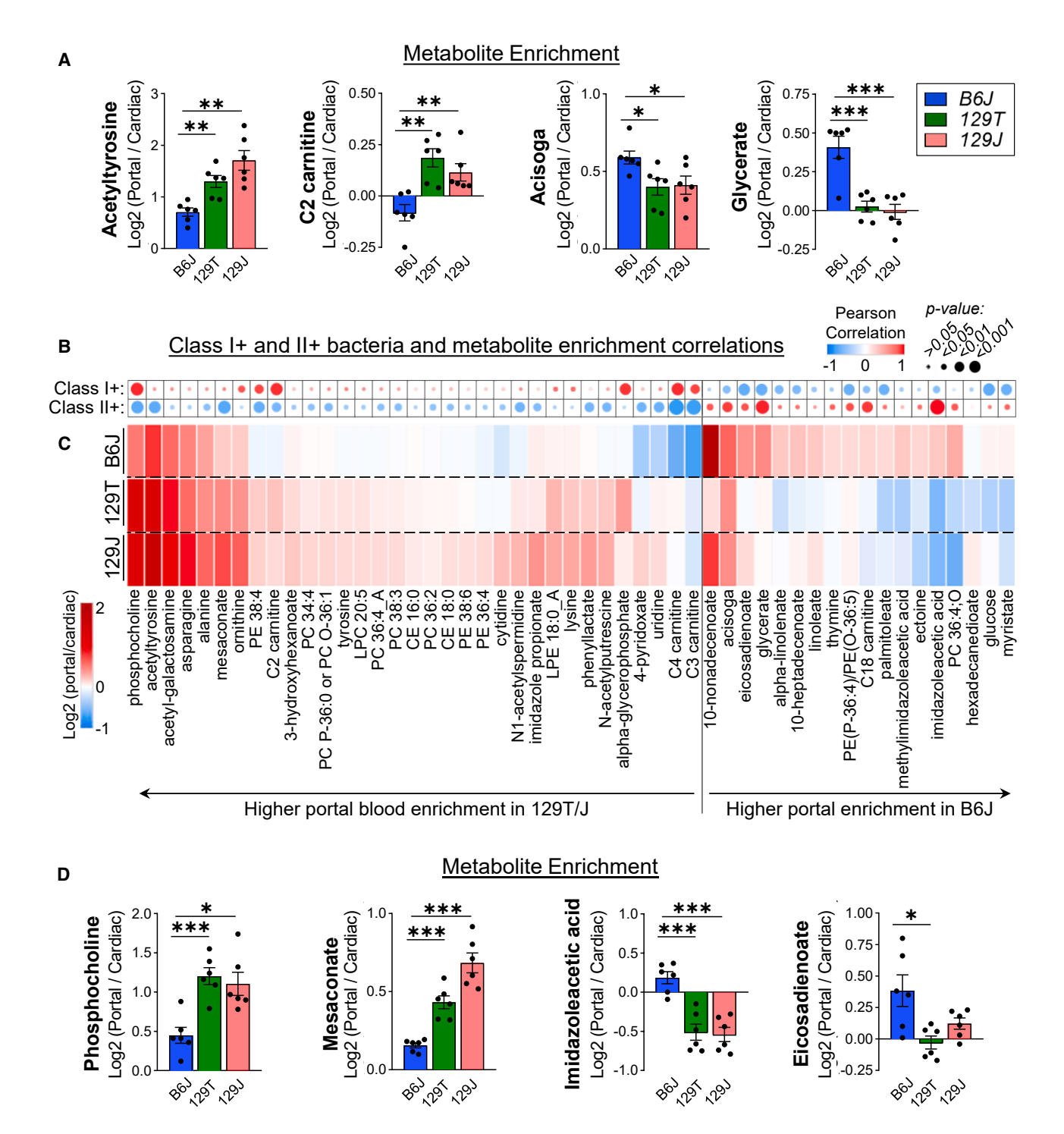


Figure 5. Class I+ and II+ bacteria species correlated with portal metabolite enrichment

(A) \log_2 of the ratio of portal abundance/cardiac abundance (left) for acetyltyrosine, C2 carnitine, acisoga, and glycerate in B6J, 129T, and 129J mice. (B and C) (B) Positive (red) or negative (blue) correlation of class I+ and II+ bacteria species with metabolite enrichment (C) in the portal and cardiac blood of B6J, 129T, and 129J represented in the heatmap.

(D) \log_2 of the ratio of portal abundance/cardiac abundance (left) for phosphocholine, mesaconate, imidazoleacetic acid, and eicosadienoate in B6J, 129T, and 129J mice. Data are expressed as mean \pm SEM (*p < 0.05, **p < 0.01, ***p < 0.001; unpaired t test for comparison between conditions).

we correlated average levels of these microbiota with portal versus cardiac enrichment of individual metabolites across all three strains of mice on HFD (Figure 5B). Of the measured metabolites with significant correlation, 33 showed higher portal enrichment in 129 compared with B6J mice, while 18 showed greater portal enrichment in B6J mice (Figure 5C). In general,



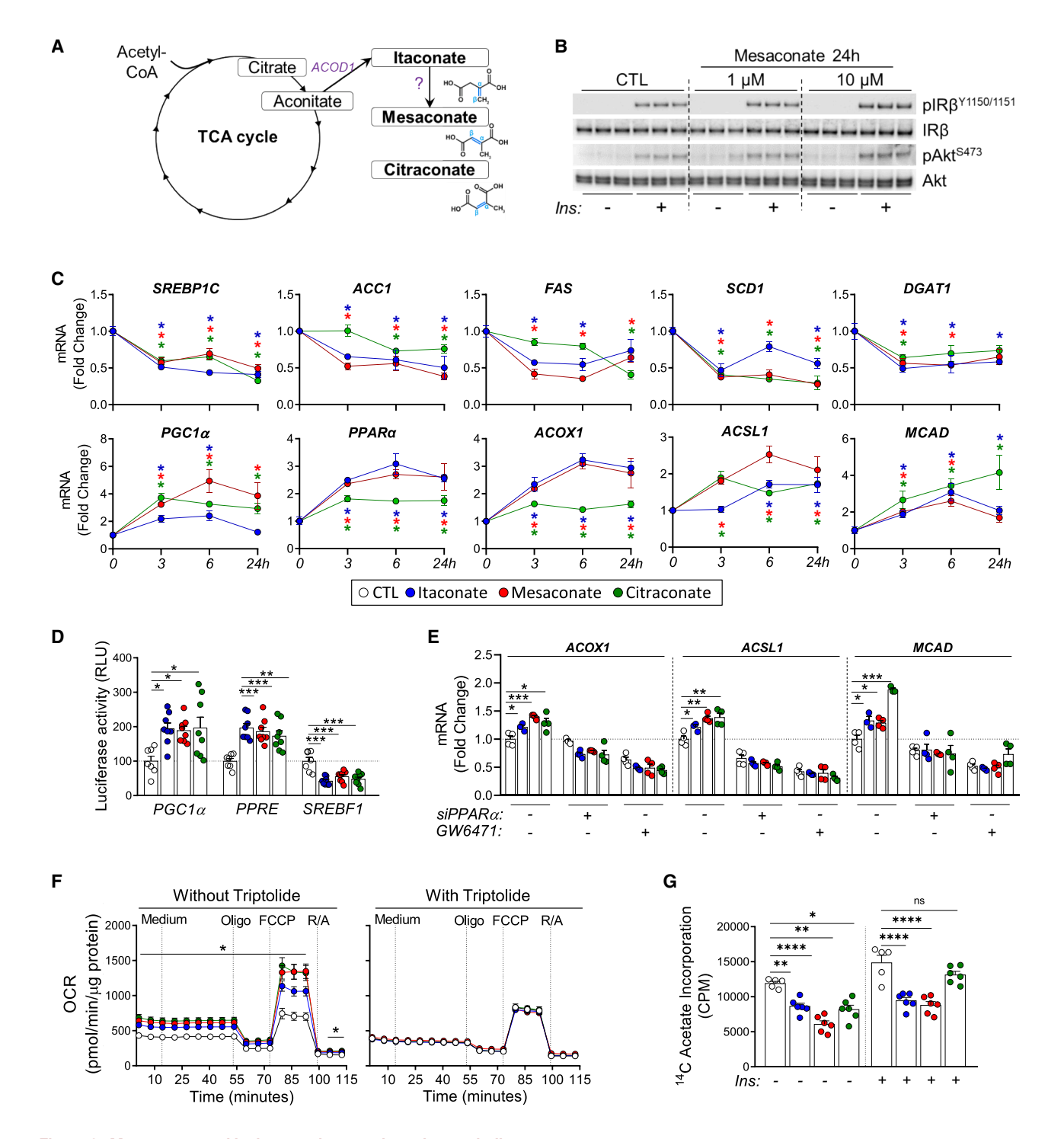


Figure 6. Mesaconate and its isomers improve hepatic metabolism

(A) Schematic representation of TCA cycle intermediates to generate itaconate, mesaconate, and citraconate. (B) $pIR\beta^{Y1150/Y1151}$ phosphorylation and $pAkt^{S473}$ phosphorylation following insulin-stimulation (100 nM) of HepG2 cells treated with 1 or 10 μ M mesaconate for 24 h.

(C) Time course (3, 6, and 24 h) of expression of lipogenic genes (SREBP1C, ACC1, FAS, SCD1, and DGAT1) and fatty acid oxidation genes (PGC1 α , PPAR α , ACOX1, ACSL1, and MCAD) in HepG2 cells following treatment with 10 μ M itaconate (blue line), mesaconate (red line), or citraconate (green line). Gene expression was normalized to the level of the Actb gene. The asterisk (*) indicates a significant difference of that time point to the 0 h time point, using the color code indicated above.

(D) Luciferase assay of PGC1 α proximal promoter, PPAR response elements, and SREBF1 response elements in HepG2 cells treated with itaconate, mesaconate, and citraconate (10 μ M, for 6 h).



Cell MetabolismArticle

metabolites with higher portal enrichment in 129 mice positively correlated with abundance of class I+ bacteria and negatively correlated with class II+ bacteria (Figure 5B). For some metabolites, e.g., 4-pyridoxate, uridine, and C3/C4 carnitines, there was strain switching of enrichment, being cardiac enriched in B6J mice but portally enriched in 129 strains (Figure 5C). Conversely, glycerate, alpha-linolenate, thymine, palmitoleate, ectoine, and imidazoleacetic acid were portally enriched in B6J mice but cardiac enriched in 129T/129J (Figure 5C), indicating differences in extraction/addition of metabolites by the liver in the three mouse strains. In every case, metabolites with higher portal enrichment in B6J mice negatively correlated with class I+ bacteria and positively correlated with class II+ bacteria (Figures 5B and 5C). Other metabolites with higher portal enrichment in 129 versus B6J mice included phosphocholine and mesaconate (Figures 5C, 5D, and S4D), while metabolites that exhibited higher portal enrichment in B6J versus 129 mice included imidazoleacetic acid and eicosadienoate (Figures 5C, 5D, and S4D). Several metabolites with higher portal enrichment in 129 showed negative correlations with body weight, HOMA-IR, and lipogenic gene expression and positive correlations with hepatic Igfbp2 mRNA levels (Figure S4E). By contrast, metabolites with higher portal enrichment in B6J showed positive correlations with body weight, HOMA-IR, and lipogenic gene expression, and negative correlations with Igfbp2 mRNA levels (Figure S4E). Thus, metabolites showing higher portal levels and portal enrichment in 129J/ 129T mice were associated with a better metabolic phenotype, whereas metabolites enriched in the portal blood of B6J mice were associated with a worse metabolic phenotype.

Mesaconate and its isomers modulate hepatic metabolism and gene expression

Metabolomics from antibiotic (especially vancomycin)-treated HFD-B6J mice and 129J/129T strains that have increased insulin sensitivity and lower risk of metabolic syndrome revealed several TCA-cycle-derived intermediates, e.g., aconitate and mesaconate, to be enriched in portal blood (Figures 3A, 5D, and S4D). We hypothesized that these metabolites act as intermediates between the microbiome or microbiome effects on hepatic insulin action and metabolic regulation (Figure 6A). We therefore tested the effects of these metabolites on signaling and gene expression in HepG2 hepatocytes, focusing on concentrations within the physiological range. Interestingly, all three metabolites improved IR and Akt phosphorylation, with 10 μM mesaconate increasing pIR_β^{Y1150/Y1151} phosphorylation by 31% and pAkt^{S473} phosphorylation by 80% (Figures 6B and S6A-S6C). All three metabolites also reduced mRNA levels of the major upstream regulators of lipid metabolism, SREBP1C, CHREBP, and LXRβ, by 30%-60%, with smaller reductions in SREBP1A and LXR α (Figures 6C, S6D, and S6E) at 3-24 h. Importantly, this was accompanied by 25%-76% downregulation of downstream genes for *de novo* lipogenesis, including *ACC1*, *FAS*, *SCD1*, and *DGAT1* (Figure 6C), as well as the long-chain fatty acid transporters *CD36* and *FATP1*. These reductions were paralleled by reductions in protein content (Figure S6F).

At the same time, mesaconate and its isomers led to 2- to 3-fold increases in expression of $PGC1\alpha$, $PPAR\alpha$, ACOX1, ACSL1, and MCAD, reflecting increased fatty acid oxidation (Figure 6C, bottom), and upregulation of SREBP2, a key regulator of cholesterol metabolism, and its target genes HMGCS, SQLE, and ACAT1 (Figures S6D and S6E). Upregulation of $PPAR\alpha$ and ACSL1 in response to metabolites was confirmed at the protein level (Figure S6F). Although no metabolite produced changes in FOXO1 expression, itaconate, mesaconate, and to a lesser extent, citraconate produced upregulation of PCX, PK, and PDHA genes (Figures S6D and S6E). Interestingly, several genes involved in glucose metabolism, including G6PC, PCK1, and PK, were downregulated by citraconate but upregulated 1.6- to 2.2-fold by itaconate or mesaconate (Figures S6D and S6E). The changes are summarized in Figure S6E, indicating upregulation of genes of fatty acid oxidation/glucose metabolism and downregulation of genes of de novo lipogenesis and their respective transcription factors by itaconate, mesaconate, and citraconate. These effects were blocked by the inhibitor of transcription triptolide (Figure S7A). Consistent with this, treatment of HepG2 cells with these metabolites increased luciferase activity of the PGC1α proximal promoter and PPAR response elements, while decreasing activity of a reporter plasmid under control of the sterol-responsive element SREBF1, with no changes on LXR activity (Figure 6D). Metabolite treatment after small interfering RNA (siRNA) knockdown of PPAR α or a PPAR α antagonist led to an \sim 60% decrease in PPAR α expression (Figure S7B) and loss of metabolite effects to upregulate ACOX1, ACSL1, and MCAD (Figure 6E), confirming that these effects were dependent on PPAR α .

These changes in gene expression induced by mesaconate and its isomers altered mitochondrial function. Thus, mitochondrial membrane potential in HepG2 cells was upregulated by treatment with 10 μM itaconate or citraconate and trended to be increased by mesaconate (Figure S7C). In addition, when AML12 hepatocytes were treated with these three metabolites, all enhanced basal oxygen consumption and maximal respiration in response to carbonyl cyanide-4-(trifluoromethoxy)phenylhydrazone (FCCP) (Figure 6F). This improved mitochondrial function was accompanied by lower acetate incorporation under both starvation and insulin-stimulated conditions, consistent with reduced de novo lipogenesis (Figure 6G). As with gene expression, these effects were lost when transcription was inhibited with triptolide (Figure 6F). Additionally, the effects of the metabolites on mitochondrial oxidation were diminished when cells were treated with a mitochondrial pyruvate carrier

⁽E) Expression of genes downstream of PPAR α (ACOX1, ACSL1, and MCAD) in HepG2 cells transfected with a control non-targeting siRNA (siNT), siPPAR α (5 pmol/well, 48 h), and PPAR α antagonist (GW6471, 10 μ M, 24 h). Expression was normalized to the level of the Actb gene. The cells were transfected 48 h before collection, and the antagonist was added 24 h before collection. In the last 6 h, cells were treated with the metabolites at 10 μ M for 6 h.

⁽F) Oxygen consumption rate of AML12 hepatocytes pretreated with itaconate, mesaconate, and citraconate (10 μ M, for 6 h). A parallel set of cells was pretreated with triptolide (TPL, 100 nM, for 2 h) prior to treatment with itaconate, mesaconate, and citraconate.

⁽G) 14 C-Acetate incorporation in HepG2 cells after serum starvation or insulin treatment (100 nM, for 6 h) in combination with itaconate, mesaconate, and citraconate treatment at 10 μ M for 6 h. Data are expressed as mean \pm SEM (*p < 0.05, **p < 0.01, ***p < 0.001; one-way ANOVA followed by Tukey's post test).

Article



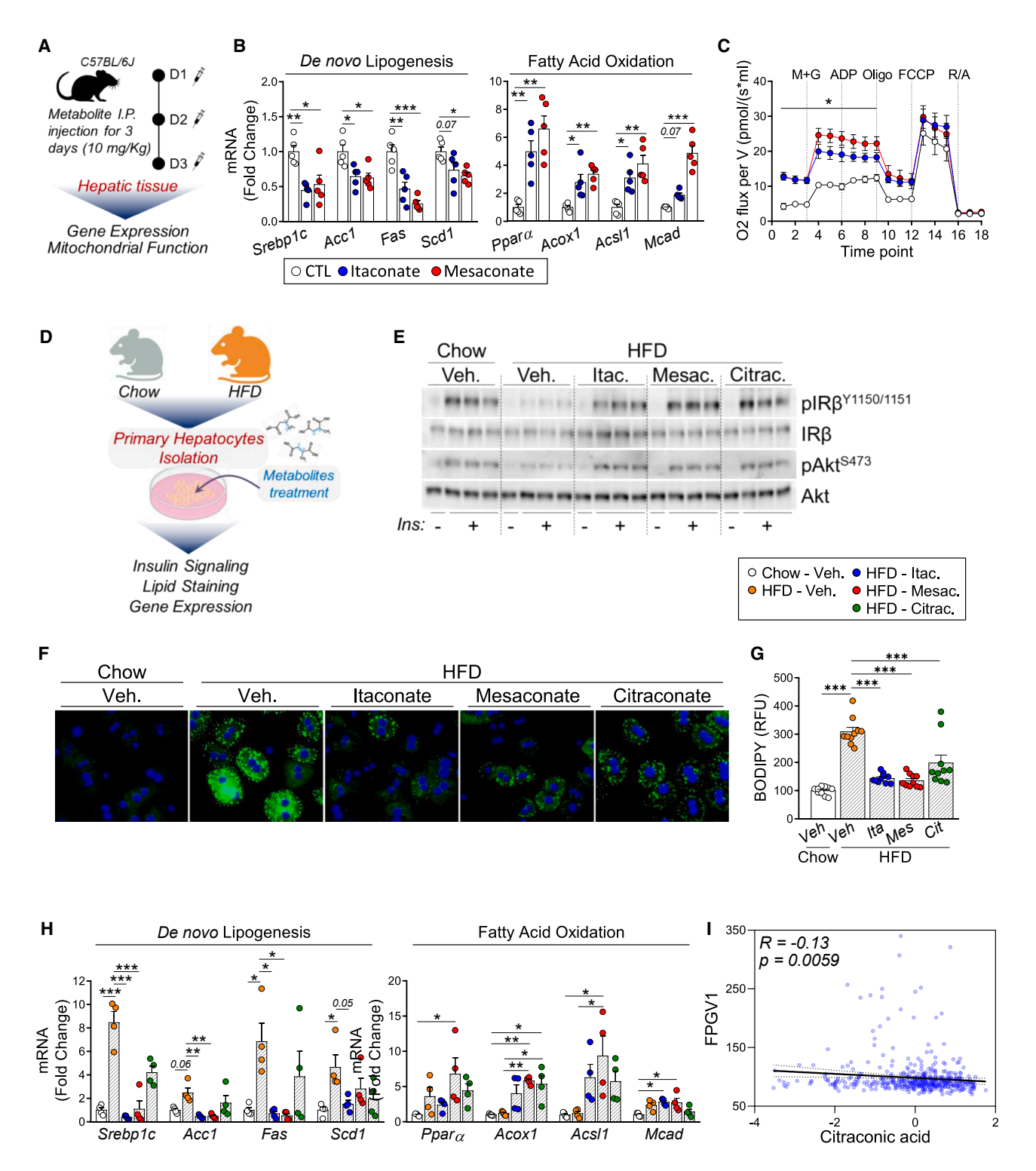


Figure 7. Mesaconate and its isomers correct insulin resistance in hepatocytes

(A) Schematic of itaconate and mesaconate *in vivo* treatment. Male C57BL/6J (B6J) at 8 weeks old on a chow diet were intraperitoneally (i.p.) injected for 3 consecutive days. Liver was collected 6 h after the last injection for analysis of gene expression and mitochondrial function.

(B) Expression of de novo lipogenesis genes (Srebp1c, Acc1, Fas, and Scd1) and FAO genes (Ppara, Acox1, Acsl1, and Mcad) was assessed by real-time qPCR normalized to the level of the Actb gene.

(C) Mitochondrial function of liver lysates from itaconate- and mesaconate-treated mice in response to malate + glutamate (M + G), ADP, oligomycin, FCCP, and rotenone/antimycin a (R/A) was assessed by Oroboros.

(D) Schematic of metabolite treatment in primary hepatocytes derived from chow- or HFD-fed mice.



inhibitor (Figure S7D), consistent with a role of glycolytic capacity in this effect (Figure S7E). Again, these effects were blocked by pretreatment with the transcription inhibitor triptolide (Figure S7F).

Mesaconate and its isomers improve hepatic metabolism *in vivo* and correct insulin resistance

To determine if the effects observed *in vitro* occur *in vivo*, we treated B6J mice with itaconate or mesaconate (10 mg/kg intraperitoneally) for 3 days (Figure 7A) and assessed gene expression and mitochondrial metabolism. Recapitulating the *in vitro* effects, *in vivo* treatment of mice with itaconate/mesaconate reduced hepatic expression of Srebp1c, as well as genes involved in *de novo* lipogenesis, by $\sim 50\%$ (Figure 7B). At the same time, expression of Ppar α and its downstream genes involved in fatty acid oxidation was upregulated by 5- to 6-fold (Figure 7B). These effects were accompanied by increased oxidative activity, as well as responses to malate and glutamate, in isolated mitochondria from both the itaconate- and mesaconate-treated mice (Figures 7C and S7G). Thus, itaconate and mesaconate at physiological concentrations can regulate hepatic gene expression and function both *in vitro* and *in vivo*.

To investigate the effects of mesaconate isomers under pathological conditions, we isolated hepatocytes from chow- and HFD-fed B6J mice and metabolite treated them in vitro (Figure 7D). Primary hepatocytes from HFD-fed mice exhibited marked insulin resistance with reduced insulin-stimulated phosphorylation of IRβ^{Y1150/Y1151} and Akt^{S473} compared with hepatocytes from chow-fed mice (Figures 7E and S7H). Treatment of these insulin-resistant hepatocytes with itaconate, mesaconate, or citraconate restored insulin sensitivity to levels observed in chow-fed mice (Figures 7E and S7H). This was accompanied by a reduction in intracellular lipid content (Figures 7F and 7G), reflecting transcriptional reprogramming by mesaconate isomers that promotes a reduction in de novo lipogenesis and enhances fatty acid oxidation (Figure 7H). Finally, in samples from the Jackson Heart Study, a large, community-based study trying to identify risk factors for heart disease in African Americans, there was a significant negative correlation between citraconate levels and fasting glucose $(\beta = -3.508, p = 0.017)$ (Figure 71), suggesting that these metabolites may exert beneficial effects on cardiometabolic health in humans as well.

DISCUSSION

The gut microbiome is a major contributor to health and disease through multiple mechanisms, including effects on intestinal integrity, regulation of inflammation, and contributions to circu-

lating metabolites through the actions of the bacteria on dietary constituents. 34-36 These factors can be modulated by the nature of the diet, composition of the microbiome, and host genetics. The portal vein drains blood from the intestine, 21 making the liver the first site of impact of gut microbiota-derived metabolites. Here, we have explored this interaction by assessing portal versus peripheral serum metabolites in strains of mice with different propensities to metabolic syndrome on chow and HFDs, as well as metabolic syndrome-prone B6J mice on HFD without/with antibiotic treatment. We show that the metabolomic profile in portal blood is quantitatively and qualitatively distinct from that in cardiac blood and that this relationship changes differently in different strains of mice and in response to diet/antibiotics. More importantly, these differences can be used to identify metabolites that have potent effects on hepatic insulin action and gene expression.

In obesity/diabetes-prone C57B/6J mice, many bile acids, N-acetylated amino acids, citrulline, and TCA cycle-related metabolites are significantly enriched in portal versus peripheral blood, indicating that the gut/gut microbiota are important contributors to the circulating levels of these metabolites. By contrast, nucleosides, cholesteryl esters, and essential fatty acids are enriched in cardiac blood, suggesting a role of the liver and other tissues in contributing these to the circulation. HFD induces major changes in the portal/cardiac blood metabolomic profiles. However, the nature of these changes is not always intuitive. For example, lipids are enriched in portal or peripheral blood depending on the species. SCFAs, which are known bacterial metabolites, 17 are enriched in portal blood, while cholesteryl esters and essential fatty acids are enriched in cardiac blood. Some of these differences may relate to the pathway of entry of the metabolite into the circulation. 37,38 SCFAs/medium-chain fatty acids present in the gut are taken up directly into the portal circulation, whereas long-chain fatty acids and many triglycerides are incorporated into chylomicrons and absorbed via lymphatics, entering the peripheral circulation when the thoracic duct drains into the subclavian vein. 37 Hence, the effects of HFD on portal enrichment of many TAGs can be explained by a combination of reshaping of the gut microbiome and alterations in intestinal lipid absorption. 39 Indeed, lipid absorption in germ-free mice is reduced as compared with conventional mice, and this contributes to their relative resistance to diet-induced obesity.40

Besides lipids, N-acetylated amino acids show portal enrichment, which is affected by HFD. N-acetylation is a common protein modification, ⁴¹ which has been related to Crohn's disease. ⁴² N-acetylated amino acids are less abundant in portal blood of germ-free mice, ⁴³ suggesting a bacterial origin. By contrast, metabolites that show cardiac blood enrichment, such as purines

⁽E) $pIR\beta^{Y1150/Y1151}$ and $pAkt^{S473}$ phosphorylation in insulin-stimulated (100 nM) primary hepatocytes treated with itaconate, mesaconate, or citraconate (10 μ M, 6 h).

⁽F) Representative images of BODIPY staining of primary hepatocytes treated with itaconate, mesaconate, or citraconate (10 μ M, 6 h).

⁽G) Quantification of relative fluorescence units (RFUs) from BODIPY staining.

⁽H) Expression of $de\ novo$ lipogenesis genes (Srebp1c, Acc1, Fas, and Scd1) and FAO genes ($Ppar\alpha$, Acox1, Acs11, and Mcad) in primary hepatocytes derived from chow- or HFD-fed mice, treated with itaconate, mesaconate, or citraconate (10 μ M, 6 h). Target gene expression was normalized to the level of the Actb gene. Data are expressed as mean \pm SEM. One-way ANOVA followed by post test Tukey's is indicated: p<0.05, p<0.01, p<0

⁽I) Correlation between fasting plasma glucose levels (FPGV1) and citraconic acid in humans in the Jackson Heart Study (JHS) cohort.

Article



(xanthine and hypoxanthine) and pyrimidine (uracil), as well as nucleosides (uridine and thymidine) and nucleotides, such as AMP, can all be produced by the liver, leading to enrichment in cardiac versus portal blood.⁴⁴

To define the effects of the microbiome, host genetics, and diet on the portal metabolome, we integrated data comparing the effects of HFD on metabolic syndrome-prone B6J mice to metabolic syndrome-resistant 129J/129T mice and data on HFD-fed B6J mice treated with antibiotics, which are potent modifiers of the microbiome known to improve insulin resistance. 9,28,29 Combining these cohorts, we identified two classes of gut microbiota: class I+, associated with metabolic benefit (higher in 129 than B6J mice and upregulated in B6J by antibiotics), versus class II+ microbes that were metabolically detrimental (low in 129 versus B6J and attenuated in B6J by antibiotics). Class I+ microbes include L. bacterium A4, B. uniformis, M. schaedleri, L. murinus, D. sp5-2, and O. sp 1-3, while class II+ includes D. newyorkensis, L. johnsonii, L. bacterium 28-4, and E. caecimuris. Metagenomes of class II+ metabolically detrimental bacteria reveal high levels of genes involved in ketogenesis, galactose/phenylalanine degradation, and peptidoglycan biosynthesis, whereas class I+ metabolically beneficial microbes showed enrichment of pathways for lysine/tryptophan/isoleucine biosynthesis, gluconeogenesis, and glycolysis.

Correlating these bacterial classes with metabolite enrichment reveals 18 metabolites that show higher portal enrichment in B6J mice and a positive association with insulin resistance, including eicosadienoate, glycerate, thymine, ectoine, imidazole-acetic acid, and methionine sulfoxide. By contrast, 33 metabolites are enriched in portal blood of mice with low risk of metabolic syndrome (129 mice and HFD-B6J mice on antibiotics) and positively correlate with markers of insulin sensitivity, including phosphocholine, acetyltyrosine, alanine, C2/C3/C4 carnitine, and mesaconate. Among these, phosphocholine has been previously associated with higher insulin sensitivity, ⁴⁵ and alanine supplementation has been shown to improve insulin sensitivity in humans.

The most striking finding, however, is the presence of higher portal levels and portal enrichment of multiple TCA cycle metabolites associated with the insulin-sensitive state. Although both gut bacteria and host intestinal cells use the TCA cycle in their normal metabolism,47 this finding is most prominent in HFD mice treated with vancomycin and correlates with gut microbiota showing enrichment of TCA cycle-related enzymes. It is important to keep in mind that while some microbiota have a full complement of genes required for the TCA cycle, some bacteria express genes for only a few of the enzymes of the cycle, allowing accumulation of different TCA metabolites, 47 and others utilize reverse Krebs/TCA cycle reactions to produce carbon compounds from carbon dioxide.⁴⁸ In addition, it is possible that different gut bacterial species and their metabolites regulate intestinal metabolism⁴⁹⁻⁵² and hence its metabolite production. This may also vary in different regions of the gut, as exemplified by selective upregulation of several TCA cycle enzymes in the colon of the vancomycin group.

Finding portal enrichment of multiple TCA cycle metabolites (citrate/isocitrate, aconitate, mesaconate, fumarate/maleate, and 2-hydroxyglutarate) associated with insulin sensitivity suggests that portal enrichment of these metabolites may positively influence hepatic metabolism. Indeed, when hepatocytes are

incubated with physiological concentrations of mesaconate and its isomers, we observe reduced expression of multiple genes related to *de novo* lipogenesis, including their upstream transcription factors. In addition, these metabolites increased expression of $PGC1\alpha$, $PPAR\alpha$, and downstream genes involved in fatty acid oxidation. These changes are associated with reduced acetate incorporation into lipids, enhanced mitochondrial function, and increased glycolytic capacity. All of these effects are mediated by transcriptional processes and blocked by triptolide or knockdown of upstream transcriptional regulators.

Recently, mesaconate, itaconate, and citraconate have been shown to suppress LPS-induced gene expression in macrophages, reduce cytokine/chemokine release, and reduce oxidative stress, all of which would improve insulin sensitivity. 53-55 Itaconate has also been shown to increase fatty acid oxidation through stabilization of CPT1a,56 protect against oxidative stress,⁵⁷ and enhance the ability of hepatocytes to metabolize fatty acids.58 We find that mice treated with itaconate/mesaconate show a reduction of de novo lipogenesis genes, increases in genes of fatty acid oxidation in the liver, and improved mitochondrial function. Importantly, when primary hepatocytes are isolated from HFD-fed mice, treatment with mesaconate and its isomers rescues insulin signaling to chow-fed levels, decreases lipid accumulation, and normalizes expression of genes related to de novo lipogenesis and fatty acid oxidation. In addition, in human population studies, citraconate levels are negatively correlated with multiple measures of metabolic syndrome, including BMI, fasting glucose, and triglycerides. Thus, these TCA-cycle-related intermediates are not just markers of metabolic syndrome but can also serve as regulators of metabolism. Determining the exact source of portal metabolites is challenging, since in addition to gut bacteria producing metabolites, the intestine is metabolically active⁵⁹⁻⁶¹ and may also be regulated by gut bacteria. 49-52

In conclusion, metabolites exhibit significant differences in level in portal versus peripheral blood. This differs among mouse strains, as well as following HFD and/or antibiotic treatment. In many cases, these affect portal levels of the metabolite with little or no change in concentration in the systemic circulation. These portal metabolites can affect hepatic metabolism and metabolic phenotype. Indeed, the TCA cycle intermediate mesaconate and its isomers are strong regulators of hepatic insulin signaling and gene expression, enhancing hepatic fatty acid oxidation and reducing *de novo* lipogenesis. Identification of regulatory metabolites provides new insights into the mechanisms by which gut microbiota regulate host metabolism and the opportunity to use these to protect from the development of or treat metabolic syndrome.

Limitations of the study

This study provides important advances in understanding how gut microbiota influence hepatic metabolism via portal-circulating metabolites; however, the precise origin of these metabolites remains to be determined, since both gut bacteria and enterocytes are metabolically active and share many pathways. Moreover, microbial composition and gene expression vary in different regions of the gastrointestinal tract, making it challenging to pinpoint the exact location of metabolite production. Future studies should aim to identify specific genes within





defined bacterial taxa linked to the production of these metabolites, thereby enabling more targeted strategies to manipulate their levels. In addition, metabolite levels are in constant flux, and the metabolomics analysis was done at only one time point (2 h fast in mice). Fasting, refeeding, and differing nutrients in the diet will certainly modulate the enrichment of metabolites in the portal and cardiac circulation. It is also important to keep in mind that improvement in metabolism can be the result of multiple factors. Indeed, although treatment with either vancomycin or metronidazole improved metabolic function, the enrichment of TCA cycle-related metabolites in the portal blood and increased TCA cycle enzymatic activity in the gut microbiome were specific to the vancomycin-treated group, suggesting that metronidazole improves host insulin sensitivity through distinct mechanisms. Although we observe potent effects of itaconate and its isomers on the regulation of insulin sensitivity, gene expression, and lipogenesis/lipid oxidation, and our data indicate that these actions are dependent on transcriptional regulation via PPAR α , PGC1 α , PPAR α , and SREBF1, the precise molecular targets of these metabolites are unclear. It is possible that these metabolites directly interact with these or other proteins, altering their activity and modulating cellular function through mechanisms, including metabolic flux, post-transcriptional modification, and epigenetics. Further study will be required to define how these metabolites contribute to the improved metabolic phenotype and allow translation of this information to the clinical setting. Finally, it is important to note that the assessment of the levels of these three closely related metabolites in most mouse and human studies is very limited, with most platforms measuring only one of the three. Future studies should systematically assess all three metabolites so that one can identify which of these metabolites is likely to be having these effects.

RESOURCE AVAILABILITY

Lead contact

Requests for additional information, resources, or reagents should be addressed to the lead contact, C. Ronald Kahn: c.ronald.kahn@joslin.harvard.edu.

Materials availability

This study did not generate any new or unique reagents.

Data and code availability

This study did not produce any new code. All datasets generated or analyzed are provided within the published article. The accession numbers for the metabolomics data reported in this study are Metabolomics Workbench: ST004132 and ST004133. Additionally, all source data used to create the graphs in the manuscript are available in Data S1.

ACKNOWLEDGMENTS

We thank all Kahn lab members for their useful discussions. This work was supported by NIH grants R01DK121967, R01DK031036, and R01DK128429 (to C.R.K.); R01DK081572 (to R.E.G.); P30DK036836 (to Joslin Diabetes Center); the Mary K. Iacocca Professorship (to C.R.K.); NHLBI grant K23HL171844 (to M.Y.M.); and the FAPESP process no. 2022/05957-0 (to V.R.M.). The JHS is conducted in collaboration with Jackson State University (HHSN268201800013I), Tougaloo College (HHSN268201800014I), the Mississippi State Department of Health (HHSN268201800015I/HHSN26800001), and the University of Mississippi Medical Center (HHSN268201800010I, HHSN268201800011I, and HHSN268201800012I) contracts from the NHLBI and the Na-

tional Institute for Minority Health and Health Disparities (NIMHD). Molecular data for the TOPMed program were supported by the NHLBI. Core support, including phenotype harmonization, data management, sample-identity quality control, and general program coordination, was provided by the TOPMed Data Coordinating Center (R01HL-120393, U01HL-120393, and contract HHSN268201800001I) and the TOPMed Centralized Omics REsource (CORE; contract HHSN268201600034I). We gratefully acknowledge the studies and participants who provided biological samples and data for TOPMed.

AUTHOR CONTRIBUTIONS

Conceptualization, V.R.M., F.M., and C.R.K.; methodology, V.R.M., F.M., J.A., H.P., J.M.D., A.K., and C.B.C.; validation, V.R.M., F.M., and C.R.K.; investigation, V.R.M., F.M., M.S., Y.W., L.-D.P., J.Z., S.Z., B.B.B., K.G., M.Y.M., R.E.G., and E.A.; writing – original draft, V.R.M., F.M., and C.R.K.; writing – review and editing, J.A., A.K., and C.R.K.; supervision, C.R.K.; funding acquisition, R.E.G. and C.R.K.

DECLARATION OF INTERESTS

The authors declare no competing interests.

STAR*METHODS

Detailed methods are provided in the online version of this paper and include the following:

- KEY RESOURCES TABLE
- EXPERIMENTAL MODEL AND STUDY PARTICIPANT DETAILS
 - o Mouse models
 - O Human data
- METHOD DETAILS
 - $\circ\,$ mRNA and qPCR analysis
 - $\,\circ\,$ DNA extraction, Library preparation and DNA sequencing
 - O Metagenomic Data Analysis
 - Gene Family Analysis and Mapping to Enzyme Commission Numbers
 - o Metabolomic library preparation and mass spectrometry analysis
 - o Cell culture
 - o Immunoblotting analysis
 - o Assessment of Mitochondrial Function
 - o In vivo treatment with itaconate and mesaconate
 - o Primary Hepatocytes Isolation
- QUANTIFICATION AND STATISTICAL ANALYSIS

SUPPLEMENTAL INFORMATION

Supplemental information can be found online at https://doi.org/10.1016/j.cmet.2025.08.005.

Received: January 21, 2025 Revised: June 23, 2025 Accepted: August 7, 2025 Published: September 5, 2025

REFERENCES

- Gurung, M., Li, Z., You, H., Rodrigues, R., Jump, D.B., Morgun, A., and Shulzhenko, N. (2020). Role of gut microbiota in type 2 diabetes pathophysiology. EBioMedicine 51, 102590. https://doi.org/10.1016/j.ebiom. 2019 11 051
- Ridaura, V.K., Faith, J.J., Rey, F.E., Cheng, J., Duncan, A.E., Kau, A.L., Griffin, N.W., Lombard, V., Henrissat, B., Bain, J.R., et al. (2013). Gut microbiota from twins discordant for obesity modulate metabolism in mice. Science 341, 1241214. https://doi.org/10.1126/science.1241214.

Article



- Van Hul, M., and Cani, P.D. (2023). The gut microbiota in obesity and weight management: microbes as friends or foe? Nat. Rev. Endocrinol. 19, 258–271. https://doi.org/10.1038/s41574-022-00794-0.
- Liu, B.N., Liu, X.T., Liang, Z.H., and Wang, J.H. (2021). Gut microbiota in obesity. World J. Gastroenterol. 27, 3837–3850. https://doi.org/10.3748/ wjg.v27.i25.3837.
- Cunningham, A.L., Stephens, J.W., and Harris, D.A. (2021). Gut microbiota influence in type 2 diabetes mellitus (T2DM). Gut Pathog. 13, 50. https:// doi.org/10.1186/s13099-021-00446-0.
- Cani, P.D., Depommier, C., Derrien, M., Everard, A., and de Vos, W.M. (2022). Akkermansia muciniphila: paradigm for next-generation beneficial microorganisms. Nat. Rev. Gastroenterol. Hepatol. 19, 625–637. https:// doi.org/10.1038/s41575-022-00631-9.
- Kootte, R.S., Levin, E., Salojärvi, J., Smits, L.P., Hartstra, A.V., Udayappan, S.D., Hermes, G., Bouter, K.E., Koopen, A.M., Holst, J.J., et al. (2017). Improvement of insulin sensitivity after lean donor feces in metabolic syndrome is driven by baseline intestinal microbiota composition. Cell Metab. 26, 611–619.e6. https://doi.org/10.1016/j.cmet.2017. 09.008.
- de Groot, P.F., Frissen, M.N., de Clercq, N.C., and Nieuwdorp, M. (2017).
 Fecal microbiota transplantation in metabolic syndrome: History, present and future. Gut Microbes 8, 253–267. https://doi.org/10.1080/19490976.
 2017 1293224
- Ussar, S., Griffin, N.W., Bezy, O., Fujisaka, S., Vienberg, S., Softic, S., Deng, L., Bry, L., Gordon, J.I., and Kahn, C.R. (2015). Interactions between gut microbiota, host genetics and diet modulate the predisposition to obesity and metabolic syndrome. Cell Metab. 22, 516–530. https://doi. org/10.1016/j.cmet.2015.07.007.
- Obata, Y., Castaño, Á., Boeing, S., Bon-Frauches, A.C., Fung, C., Fallesen, T., de Agüero, M.G., Yilmaz, B., Lopes, R., Huseynova, A., et al. (2020). Neuronal programming by microbiota regulates intestinal physiology. Nature 578, 284–289. https://doi.org/10.1038/s41586-020-1975-8.
- Allam-Ndoul, B., Castonguay-Paradis, S., and Veilleux, A. (2020). Gut microbiota and intestinal trans-epithelial permeability. Int. J. Mol. Sci. 21, 6402. https://doi.org/10.3390/ijms21176402.
- Clarke, G., Stilling, R.M., Kennedy, P.J., Stanton, C., Cryan, J.F., and Dinan, T.G. (2014). Minireview: Gut microbiota: the neglected endocrine organ. Mol. Endocrinol. 28, 1221–1238. https://doi.org/10.1210/me. 2014-1108.
- de Vos, W.M., Tilg, H., Van Hul, M., and Cani, P.D. (2022). Gut microbiome and health: mechanistic insights. Gut 71, 1020–1032. https://doi.org/10. 1136/gutinl-2021-326789.
- Koh, A., and Bäckhed, F. (2020). From association to causality: the role of the gut microbiota and its functional products on host metabolism. Mol. Cell 78, 584–596. https://doi.org/10.1016/j.molcel.2020.03.005.
- 15. Chiang, J.Y.L. (2013). Bile acid metabolism and signaling. Compr. Physiol. 3, 1191–1212. https://doi.org/10.1002/cphy.c120023.
- Ridlon, J.M., Kang, D.J., Hylemon, P.B., and Bajaj, J.S. (2014). Bile acids and the gut microbiome. Curr. Opin. Gastroenterol. 30, 332–338. https:// doi.org/10.1097/MOG.00000000000057.
- 17. den Besten, G., Bleeker, A., Gerding, A., van Eunen, K., Havinga, R., van Dijk, T.H., Oosterveer, M.H., Jonker, J.W., Groen, A.K., Reijngoud, D.J., et al. (2015). Short-chain fatty acids protect against high-fat diet-induced obesity via a PPARgamma-dependent switch from lipogenesis to fat oxidation. Diabetes 64, 2398–2408. https://doi.org/10.2337/db14-1213.
- Kondo, T., Kishi, M., Fushimi, T., and Kaga, T. (2009). Acetic acid upregulates the expression of genes for fatty acid oxidation enzymes in liver to suppress body fat accumulation. J. Agric. Food Chem. 57, 5982–5986. https://doi.org/10.1021/jf900470c.
- Weitkunat, K., Schumann, S., Nickel, D., Kappo, K.A., Petzke, K.J., Kipp, A.P., Blaut, M., and Klaus, S. (2016). Importance of propionate for the repression of hepatic lipogenesis and improvement of insulin sensitivity

- in high-fat diet-induced obesity. Mol. Nutr. Food Res. 60, 2611–2621. https://doi.org/10.1002/mnfr.201600305.
- Müller, M., Hernández, M.A.G., Goossens, G.H., Reijnders, D., Holst, J.J., Jocken, J.W.E., van Eijk, H., Canfora, E.E., and Blaak, E.E. (2019). Circulating but not faecal short-chain fatty acids are related to insulin sensitivity, lipolysis and GLP-1 concentrations in humans. Sci. Rep. 9, 12515. https://doi.org/10.1038/s41598-019-48775-0.
- Deleu, S., Arnauts, K., Deprez, L., Machiels, K., Ferrante, M., Huys, G.R.B., Thevelein, J.M., Raes, J., and Vermeire, S. (2023). High acetate concentration protects intestinal barrier and exerts anti-inflammatory effects in organoid-derived epithelial monolayer cultures from patients with ulcerative colitis. Int. J. Mol. Sci. 24, 768. https://doi.org/10.3390/ijms24010768.
- Wu, L., Tang, Z., Chen, H., Ren, Z., Ding, Q., Liang, K., and Sun, Z. (2021). Mutual interaction between gut microbiota and protein/amino acid metabolism for host mucosal immunity and health. Anim. Nutr. 7, 11–16. https:// doi.org/10.1016/j.aninu.2020.11.003.
- Schugar, R.C., Shih, D.M., Warrier, M., Helsley, R.N., Burrows, A., Ferguson, D., Brown, A.L., Gromovsky, A.D., Heine, M., Chatterjee, A., et al. (2017). The TMAO-producing enzyme flavin-containing monooxygenase 3 regulates obesity and the beiging of white adipose tissue. Cell Rep. 19, 2451–2461. https://doi.org/10.1016/j.celrep.2017.05.077.
- Stefater, M.A., Pacheco, J.A., Bullock, K., Pierce, K., Deik, A., Liu, E., Clish, C., and Stylopoulos, N. (2020). Portal venous metabolite profiling after RYGB in male rats highlights changes in gut-liver axis. J. Endocr. Soc. 4, bvaa003. https://doi.org/10.1210/jendso/bvaa003.
- Ma, Z., Huang, Z., Zhang, C., Liu, X., Zhang, J., Shu, H., Ma, Y., Liu, Z., Feng, Y., Chen, X., et al. (2023). Hepatic Acat2 overexpression promotes systemic cholesterol metabolism and adipose lipid metabolism in mice. Diabetologia 66, 390–405. https://doi.org/10.1007/s00125-022-05829-9.
- Ali, R.O., Quinn, G.M., Umarova, R., Haddad, J.A., Zhang, G.Y., Townsend, E.C., Scheuing, L., Hill, K.L., Gewirtz, M., Rampertaap, S., et al. (2023). Longitudinal multi-omics analyses of the gut-liver axis reveals metabolic dysregulation in hepatitis C infection and cirrhosis. Nat. Microbiol. 8, 12–27. https://doi.org/10.1038/s41564-022-01273-y.
- Carneiro, C., Brito, J., Bilreiro, C., Barros, M., Bahia, C., Santiago, I., and Caseiro-Alves, F. (2019). All about portal vein: a pictorial display to anatomy, variants and physiopathology. Insights Imaging 10, 38. https://doi.org/10.1186/s13244-019-0716-8.
- Fujisaka, S., Avila-Pacheco, J., Soto, M., Kostic, A., Dreyfuss, J.M., Pan, H., Ussar, S., Altindis, E., Li, N., Bry, L., et al. (2018). Diet, genetics, and the gut microbiome drive dynamic changes in plasma metabolites. Cell Rep. 22, 3072–3086. https://doi.org/10.1016/j.celrep.2018.02.060.
- Fujisaka, S., Ussar, S., Clish, C., Devkota, S., Dreyfuss, J.M., Sakaguchi, M., Soto, M., Konishi, M., Softic, S., Altindis, E., et al. (2016). Antibiotic effects on gut microbiota and metabolism are host dependent. J. Clin. Invest. 126, 4430–4443. https://doi.org/10.1172/JCl86674.
- Luo, P., and Wang, M.H. (2011). Eicosanoids, β-cell function, and diabetes. Prostaglandins Other Lipid Mediat. 95, 1–10. https://doi.org/10.1016/j.prostaglandins.2011.06.001.
- Tuomisto, K., Palmu, J., Long, T., Watrous, J.D., Mercader, K., Lagerborg, K.A., Andres, A., Salmi, M., Jalkanen, S., Vasan, R.S., et al. (2022). A plasma metabolite score of three eicosanoids predicts incident type 2 diabetes: a prospective study in three independent cohorts. BMJ Open Diabetes Res. Care 10, e002519. https://doi.org/10.1136/bmjdrc-2021-002519.
- Schubert, A.M., Sinani, H., and Schloss, P.D. (2015). Antibiotic-induced alterations of the murine gut microbiota and subsequent effects on colonization resistance against Clostridium difficile. mBio 6, e00974. https://doi.org/10.1128/mBio.00974-15.
- Rauzier, C., Chartrand, D.J., Alméras, N., Lemieux, I., Larose, E., Mathieu, P., Pibarot, P., Lamarche, B., Rhéaume, C., Poirier, P., et al. (2023). Associations of insulin-like growth factor binding protein-2 with metabolic profile and hepatic fat deposition in asymptomatic men and women. Am. J. Physiol. Endocrinol. Metab. 325, E99–E105. https://doi.org/10.1152/ajpendo.00108.2023.



Cell MetabolismArticle

- Gilbert, J.A., Blaser, M.J., Caporaso, J.G., Jansson, J.K., Lynch, S.V., and Knight, R. (2018). Current understanding of the human microbiome. Nat. Med. 24, 392–400. https://doi.org/10.1038/nm.4517.
- Jandhyala, S.M., Talukdar, R., Subramanyam, C., Vuyyuru, H., Sasikala, M., and Nageshwar Reddy, D. (2015). Role of the normal gut microbiota. World J. Gastroenterol. 21, 8787–8803. https://doi.org/10.3748/wjg.v21. i29 8787
- Belkaid, Y., and Hand, T.W. (2014). Role of the microbiota in immunity and inflammation. Cell 157, 121–141. https://doi.org/10.1016/j.cell.2014. 03.011.
- Ko, C.W., Qu, J., Black, D.D., and Tso, P. (2020). Regulation of intestinal lipid metabolism: current concepts and relevance to disease. Nat. Rev. Gastroenterol. Hepatol. 17, 169–183. https://doi.org/10.1038/s41575-019-0250-7.
- Han, Y.H., Onufer, E.J., Huang, L.H., Sprung, R.W., Davidson, W.S., Czepielewski, R.S., Wohltmann, M., Sorci-Thomas, M.G., Warner, B.W., and Randolph, G.J. (2021). Enterically derived high-density lipoprotein restrains liver injury through the portal vein. Science 373, eabe6729. https:// doi.org/10.1126/science.abe6729.
- Yu, Y., Raka, F., and Adeli, K. (2019). The role of the gut microbiota in lipid and lipoprotein metabolism. J. Clin. Med. 8, 2227. https://doi.org/10.3390/ jcm8122227.
- Martinez-Guryn, K., Hubert, N., Frazier, K., Urlass, S., Musch, M.W., Ojeda, P., Pierre, J.F., Miyoshi, J., Sontag, T.J., Cham, C.M., et al. (2018). Small intestine microbiota regulate host digestive and absorptive adaptive responses to dietary lipids. Cell Host Microbe 23, 458–469.e5. https://doi.org/10.1016/j.chom.2018.03.011.
- Ree, R., Varland, S., and Arnesen, T. (2018). Spotlight on protein N-terminal acetylation. Exp. Mol. Med. 50, 1–13. https://doi.org/10. 1038/s12276-018-0116-z.
- Zhang, X., Ning, Z., Mayne, J., Yang, Y., Deeke, S.A., Walker, K., Farnsworth, C.L., Stokes, M.P., Couture, J.F., Mack, D., et al. (2020). Widespread protein lysine acetylation in gut microbiome and its alterations in patients with Crohn's disease. Nat. Commun. 11, 4120. https://doi.org/ 10.1038/s41467-020-17916-9.
- Mardinoglu, A., Shoaie, S., Bergentall, M., Ghaffari, P., Zhang, C., Larsson, E., Bäckhed, F., and Nielsen, J. (2015). The gut microbiota modulates host amino acid and glutathione metabolism in mice. Mol. Syst. Biol. 11, 834. https://doi.org/10.15252/msb.20156487.
- Ipata, P.L., Camici, M., Micheli, V., and Tozz, M.G. (2011). Metabolic network of nucleosides in the brain. Curr. Top. Med. Chem. 11, 909–922. https://doi.org/10.2174/156802611795347555.
- Chang, W., Hatch, G.M., Wang, Y., Yu, F., and Wang, M. (2019). The relationship between phospholipids and insulin resistance: From clinical to experimental studies. J. Cell. Mol. Med. 23, 702–710. https://doi.org/10.1111/jcmm.13984.
- Matthews, J.J., Dolan, E., Swinton, P.A., Santos, L., Artioli, G.G., Turner, M.D., Elliott-Sale, K.J., and Sale, C. (2021). Effect of carnosine or betaalanine supplementation on markers of glycemic control and insulin resistance in humans and animals: a systematic review and meta-analysis. Adv. Nutr. 12, 2216–2231. https://doi.org/10.1093/advances/ nmab087.
- Wang, P.H., Correia, K., Ho, H.C., Venayak, N., Nemr, K., Flick, R., Mahadevan, R., and Edwards, E.A. (2019). An interspecies malate-pyruvate shuttle reconciles redox imbalance in an anaerobic microbial community. ISME J. 13, 1042–1055. https://doi.org/10.1038/s41396-018-0333-4.
- Hügler, M., Wirsen, C.O., Fuchs, G., Taylor, C.D., and Sievert, S.M. (2005). Evidence for autotrophic CO2 fixation via the reductive tricarboxylic acid cycle by members of the epsilon subdivision of proteobacteria. J. Bacteriol. 187, 3020–3027. https://doi.org/10.1128/JB.187.9.3020-3027.2005.
- De Vadder, F., Kovatcheva-Datchary, P., Goncalves, D., Vinera, J., Zitoun,
 C., Duchampt, A., Bäckhed, F., and Mithieux, G. (2014). Microbiota-gener-

- ated metabolites promote metabolic benefits via gut-brain neural circuits. Cell *156*, 84–96. https://doi.org/10.1016/j.cell.2013.12.016.
- De Vadder, F., Kovatcheva-Datchary, P., Zitoun, C., Duchampt, A., Bäckhed, F., and Mithieux, G. (2016). Microbiota-produced succinate improves glucose homeostasis via intestinal gluconeogenesis. Cell Metab. 24, 151–157. https://doi.org/10.1016/j.cmet.2016.06.013.
- Soty, M., Gautier-Stein, A., Rajas, F., and Mithieux, G. (2017). Gut-brain glucose signaling in energy homeostasis. Cell Metab. 25, 1231–1242. https://doi.org/10.1016/j.cmet.2017.04.032.
- Sinet, F., Soty, M., Zemdegs, J., Guiard, B., Estrada, J., Malleret, G., Silva, M., Mithieux, G., and Gautier-Stein, A. (2021). Dietary fibers and proteins modulate behavior via the activation of intestinal gluconeogenesis. Neuroendocrinology 111, 1249–1265. https://doi.org/10.1159/ 000514289.
- He, W., Henne, A., Lauterbach, M., Geißmar, E., Nikolka, F., Kho, C., Heinz, A., Dostert, C., Grusdat, M., Cordes, T., et al. (2022). Mesaconate is synthesized from itaconate and exerts immunomodulatory effects in macrophages. Nat. Metab. 4, 524–533. https://doi.org/10.1038/s42255-022-00565-1.
- Chen, F., Elgaher, W.A.M., Winterhoff, M., Büssow, K., Waqas, F.H., Graner, E., Pires-Afonso, Y., Casares Perez, L., de la Vega, L., Sahini, N., et al. (2022). Citraconate inhibits ACOD1 (IRG1) catalysis, reduces interferon responses and oxidative stress, and modulates inflammation and cell metabolism. Nat. Metab. 4, 534–546. https://doi.org/10.1038/ s42255-022-00577-x.
- Chen, L.L., Morcelle, C., Cheng, Z.L., Chen, X., Xu, Y., Gao, Y., Song, J., Li, Z., Smith, M.D., Shi, M., et al. (2022). Itaconate inhibits TET DNA dioxygenases to dampen inflammatory responses. Nat. Cell Biol. 24, 353–363. https://doi.org/10.1038/s41556-022-00853-8.
- Mainali, R., Buechler, N., Otero, C., Edwards, L., Key, C.C., Furdui, C., and Quinn, M.A. (2024). Itaconate stabilizes CPT1a to enhance lipid utilization during inflammation. eLife 12, RP92420. https://doi.org/10.7554/ eLife.92420.
- Hu, Z., Xu, D., Meng, H., Liu, W., Zheng, Q., and Wang, J. (2024). 4-octyl itaconate protects against oxidative stress-induced liver injury by activating the Nrf2/Sirt3 pathway through AKT and ERK1/2 phosphorylation. Biochem. Pharmacol. 220, 115992. https://doi.org/10.1016/j.bcp.2023. 115992.
- Weiss, J.M., Palmieri, E.M., Gonzalez-Cotto, M., Bettencourt, I.A., Megill, E.L., Snyder, N.W., and McVicar, D.W. (2023). Itaconic acid underpins hepatocyte lipid metabolism in non-alcoholic fatty liver disease in male mice. Nat. Metab. 5, 981–995. https://doi.org/10.1038/s42255-023-00801-2
- Croset, M., Rajas, F., Zitoun, C., Hurot, J.M., Montano, S., and Mithieux, G. (2001). Rat small intestine is an insulin-sensitive gluconeogenic organ. Diabetes 50, 740–746. https://doi.org/10.2337/diabetes.50.4.740.
- Tong, W., Hannou, S.A., Wang, Y., Astapova, I., Sargsyan, A., Monn, R., Thiriveedi, V., Li, D., McCann, J.R., Rawls, J.F., et al. (2022). The intestine is a major contributor to circulating succinate in mice. FASEB J. 36, e22546. https://doi.org/10.1096/fj.202200135RR.
- Jang, C., Hui, S., Lu, W., Cowan, A.J., Morscher, R.J., Lee, G., Liu, W., Tesz, G.J., Birnbaum, M.J., and Rabinowitz, J.D. (2018). The small intestine converts dietary fructose into glucose and organic acids. Cell Metab. 27, 351–361.e3. https://doi.org/10.1016/j.cmet.2017.12.016.
- Beghini, F., McIver, L.J., Blanco-Míguez, A., Dubois, L., Asnicar, F., Maharjan, S., Mailyan, A., Manghi, P., Scholz, M., Thomas, A.M., et al. (2021). Integrating taxonomic, functional, and strain-level profiling of diverse microbial communities with bioBakery 3. eLife 10, e65088. https://doi.org/10.7554/eLife.65088.
- Baym, M., Lieberman, T.D., Kelsic, E.D., Chait, R., Gross, R., Yelin, I., and Kishony, R. (2016). Spatiotemporal microbial evolution on antibiotic landscapes. Science 353, 1147–1151. https://doi.org/10.1126/science. aag0822.

Article



- Leek, J.T., and Storey, J.D. (2007). Capturing heterogeneity in gene expression studies by surrogate variable analysis. PLoS Genet. 3, 1724– 1735. https://doi.org/10.1371/journal.pgen.0030161.
- Wang, S., Ventolero, M., Hu, H., and Li, X. (2022). A revisit to universal single-copy genes in bacterial genomes. Sci. Rep. 12, 14550. https://doi.org/ 10.1038/s41598-022-18762-z.
- Kostic, A.D., Gevers, D., Siljander, H., Vatanen, T., Hyötyläinen, T., Hämäläinen, A.M., Peet, A., Tillmann, V., Pöhö, P., Mattila, I., et al. (2015). The dynamics of the human infant gut microbiome in development
- and in progression toward type 1 diabetes. Cell Host Microbe 17, 260–273. https://doi.org/10.1016/j.chom.2015.01.001.
- 67. Law, C.W., Chen, Y., Shi, W., and Smyth, G.K. (2014). voom: Precision weights unlock linear model analysis tools for RNA-seq read counts. Genome Biol. 15, R29. https://doi.org/10.1186/gb-2014-15-2-r29.
- Ritchie, M.E., Diyagama, D., Neilson, J., van Laar, R., Dobrovic, A., Holloway, A., and Smyth, G.K. (2006). Empirical array quality weights in the analysis of microarray data. BMC Bioinformatics 7, 261. https://doi. org/10.1186/1471-2105-7-261.





STAR*METHODS

KEY RESOURCES TABLE

REAGENT or RESOURCE	SOURCE	IDENTIFIER
Antibodies		
Phospho-IGF-I Receptor β (Tyr1135/1136)/Insulin Receptor β (Tyr1150/1151)	Cell Signaling	3024; RRID:AB_331253
Insulin Receptor β	Cell Signaling	3025; RRID:AB_2280448
Phospho-Akt (Ser473)	Cell Signaling	4060; RRID:AB_2315049
Akt	Cell Signaling	4685; RRID:AB_2225340
SREBP-1	Santa Cruz	SC-8984; RRID:AB_2194223
FAS	ABCAM	ab22759; RRID:AB_732316
ACC	Cell Signaling	3662; RRID:AB_2219400
PPARα	ABCAM	ab8934; RRID:AB_306869
ACSL1	Cell Signaling	9189; RRID:AB_10891616
3-actin	Santa Cruz	SC8432-HRP; RRID:AB_626630
Anti-rabbit IgG, HRP-linked Antibody	Cell Signaling	7074; RRID:AB_2099233
Anti-mouse IgG, HRP-linked Antibody	Cell Signaling	7076; RRID:AB_330924
Chemicals, peptides, and recombinant proteins		
√ancomycin	Santa Cruz	sc-224363A
Metronidazole	Sigma	M3761-25G
TRIzol Reagent	Life Technologies	15-596-018
Q SybrGreen Supermix	Bio-Rad	1708884
Mag-Bind TotalPure NGS	Omega bio-tek	M1378-00
nsulin	Millipore-Sigma	19278
taconate	Sigma	129204
Mesaconate	Sigma	131040
Ditraconate	Sigma	C82604
RIPA lysis buffer, 10X	Millipore-Sigma	20-188
Protease Inhibitor cocktail (EDTA free, 100Xin DMSO)	BioTool	B14002
Phosphatase Inhibitor Cocktail (2 Tubes, 100X)	BioTool	B15002
riptolide	MedChemExpress	HY-32735
ipofectamine 3000	ThermoFisher	L3000015
Lipofectamine RNAiMAX	ThermoFisher	13778150
PPARα antagonist, GW6471	MedChemExpress	HY-15372
SuperSignal West Pico PLUS	ThermoFisher	34580
nitochondrial pyruvate carrier (MPC) inhibitor, UK5099	Tocris	4186
MitoTracker Red FM dye	ThermoFisher	M22425
Dexamethasone	Sigma	D4902
Chloroform	ThermoFisher	AA43685K2
Oritical commercial assays		
Dual-Glo Luciferase assay system	Promega	E2940
RNeasy Mini Kit columns	QIAGEN	74106
Zymobiomics DNA miniprep kit	Zymo Research	D4300
llumina Tagment DNA TDE1 Enzyme and Buffer Kits	Illumina	20034197
Nextera DNA CD Indexes	Illumina	20018708
Pierce BCA Protein Assay Kits	ThermoFisher	23227
High-Capacity cDNA Reverse Transcription Kit	ThermoFisher	4368813

(Continued on next page)





Continued		
REAGENT or RESOURCE	SOURCE	IDENTIFIER
Experimental models: Cell lines		
HepG2 cells	ATCC	HB-8065
AML-12 cells	ATCC	CRL-2254
Primary hepatocytes	N/A	N/A
Experimental models: Organisms/strains		
Mouse: C57BL/6J	The Jackson Laboratory	000664
Mouse: 129S1/SvImJ	The Jackson Laboratory	002448
Mouse: 129S6/SvEvTac	Taconic Farms	129SVE-M
Oligonucleotides		
ON-TARGET plus Human PPARA (5465) siRNA	Horizon discovery	J-003434-05-0002
Primer sequences for quantitative RT-PCR, see Table S1	N/A	N/A
Recombinant DNA		
PGC1α proximal promoter	Addgene	154259
PPAR response elements	Addgene	1015
SREBF1 response elements	Addgene	90371
LXR response elements	Addgene	90348
pRL Renilla Luciferase Control Reporter Vector	Promega	E2261
Software and algorithms		
GraphPad Prism v8	GraphPad software	N/A
Excel	Microsoft	N/A
The R Project for Statistical Computing	https://www.r-project.org/	N/A
HUMAnN3	Beghini et al. ⁶²	N/A
Progenesis QIsoftware v2.0	Nonlinear Dynamics	N/A
TraceFinder 3.3	ThermoFisher	N/A

EXPERIMENTAL MODEL AND STUDY PARTICIPANT DETAILS

Mouse models

Male C57Bl/6J (B6J) mice were purchased from Jackson laboratory. Five-week-old mice were randomized according to body weight and housed 4 per cage. After one week of acclimation, the mice were divided into 4 groups: two groups received normal autoclaved drinking water, one received water containing vancomycin (1g/L, sc-224363A, Santa Cruz) and the fourth received water containing metronidazole (1g/L, M3761-25G, Sigma). Drinking water solutions were prepared and changed weekly. After one week, one group of mice on water continued on the regular chow diet (Mouse Diet 9F 5020, PharmaServ) while the other three groups, one on plain water and the two on antibiotics, were started on a high fat diet containing 60% fat by calories (HFD, D12492, Research Diets). All mice continued these diets from 7 to 18 weeks of age. For measurements of effect of diet/antibiotics on gene expression in intestine and liver, a second cohort was created consisting of B6J mice on either chow or HFD from ages 6 to 11 weeks without and with antibiotic supplementation in the drinking water during the last 2 weeks. To explore the role of genetic background on portal enriched metabolites, a third study group was initiated using 8-week-old mice from three different strains, B6J and 129S1 (129J) from Jackson Laboratory (Bar Harbor, ME) and 129S6 (129T) from Taconic Farms (Germantown, NY). We have previously shown^{9,28,29} that while B6J mice are both obesity and diabetes prone, 129J and 129T mice are metabolic syndrome resistant. All three strains were maintained on HFD for 12 weeks. At the end of the experiment, mice were fasted for 2 hours, anesthetized with Avertin (100 μL per 10 g of BW), after which blood samples were collected. To collect portal and cardiac blood in mice, the abdomen was opened to expose the peritoneal cavity, and the intestines were retracted to visualize the portal vein. For portal blood collection, a 27G needle attached to a 1 mL syringe was used to puncture the portal vein, and the blood was slowly. Immediately after collecting portal vein blood, an incision was made through the thoracic cavity to expose the heart. A 25G needle attached to a 1 mL syringe was inserted into the left ventricle, and as much blood as possible was withdrawn. Both portal and cardiac blood were directly transferred into collection tubes containing EDTA to obtain plasma. In addition to blood, cecal contents, intestinal and liver biopsies were collected. All experiments were approved by the IACUC of the Joslin Diabetes Center and were in accordance with NIH guidelines.

Human data

Samples from the JHS (Jackson Heart Study) — a community-based longitudinal cohort study of 5,301 self-identified Black or African American individuals from the Jackson, Mississippi, USA, metropolitan statistical area—were analyzed for plasma citraconate levels





and phenotype correlation. Here we utilized data from 466 individuals from the first exam (2000-2004) in whom citraconate was measured after being added to the metabolomics platform, assessed by liquid chromatography and mass spectrometry. The JHS study was approved by the Jackson State University, Tougaloo College, and University of Mississippi Medical Center Institutional Review Boards, and all participants provided written, informed consent.

METHOD DETAILS

mRNA and qPCR analysis

mRNA was extracted from liver, jejunum and colon in a mix of Trizol and chloroform and then precipitated with 70% of ethanol. mRNA purification was performed using RNeasy Mini Kit columns (QIAGEN, catalog 74106). cDNA was produced by reverse transcription of mRNA. qPCR was performed on CFX384 Touch Real-Time PCR Detection System, and the data were analyzed on CFX manager software (3.1, BioRad). Primers sequences are listed in the Table S1. A Kruskal-Wallis followed by a Dunn's multiple comparison was performed to identify genes differentially expressed between each group, a p-value < 0.05 was considered as significant.

DNA extraction, Library preparation and DNA sequencing

DNA was extracted from cecal samples using the Zymobiomics DNA miniprep kit (#D4300). Frozen cecal samples were homogenized in lysis solution using a bead beater homogenizer for 10 min at 20 (frequency 1/ S). The eluted genomic DNA was used as the template for the library preparation as previously described. The gDNA was standardized, tagged (Illumina Tagment DNA TDE1 Enzyme and Buffer Kits, 20034197) and PCR-mediated adaptor (Nextera DNA CD Indexes, Illumina #20018708) were incorporated into the DNA fragments and amplified. The indexed DNA libraries were cleaned with magnetic beads (Omega bio-tek, #M1378-00). The quality of the DNA libraries was assessed using a 2100 Bioanalyzer (Agilent), and the concentration of DNA read with Qubit. The 18 individual libraries were pooled, and the pooled library concentration read with Qubit and Nanodrop before being sent to Genewiz for sequencing.

Metagenomic Data Analysis

transformed value = $asin(\sqrt{proportion})$

Bacterial taxa not detected across all samples were removed, and any duplicated quantifications of the same taxa appearing at multiple taxonomic levels were filtered out. Following this, the relative abundance of each bacterial taxon was calculated as a proportion of the total bacterial community. These proportions were then arcsine-transformed using the function where 'proportion' represents the proportional abundance. Finally, the dataset was adjusted for confounding variables using surrogate variable analysis.⁶⁴

Gene Family Analysis and Mapping to Enzyme Commission Numbers

We analyzed the relative abundance of gene families in the gut microbiome of mice, focusing on those involved in the tricarboxylic acid (TCA) cycle. Initial observations utilized the UniRef90 gene family dataset, where specific enzymes linked to the TCA cycle were identified based on high abundance in the high-fat diet treated with vancomycin (HFD-Vanco) group compared to other groups. To enhance the accuracy of enzyme identification, UniRef90 gene family names were converted to the Enzyme Commission (EC) numbers as cataloged by the Nomenclature Committee of the International Union of Biochemistry and Molecular Biology (NC-IUBMB) with the use of the database conversion scripts provided in HUMAnN3. ⁶² This conversion was aimed at utilizing a curated list of non-redundant enzymes that are directly associated with specific biochemical reactions, ensuring that each enzymatic step in the TCA cycle was represented.

To address potential biases in gene abundance due to antibiotic treatment effects, we normalized the TCA cycle gene abundances against the abundances of Universal Single-Copy Genes (USCGs). ⁶⁵ These genes are typically present in a single copy per bacterial cell and serve as a benchmark for estimating the quasi-absolute abundance of genes across samples. This normalization confirmed that the observed patterns in TCA cycle gene abundances were not artifacts of relative abundance changes due to antibiotic treatment.

Metabolomic library preparation and mass spectrometry analysis LC-MS profiling

A combination of four LC-MS methods were used to profile metabolites in plasma samples as previously described ⁶⁶; two methods that measure polar metabolites, one method that measures metabolites of intermediate polarity (e.g., fatty acids and bile acids), and one method for lipid profiling. For the metabolomics analysis, samples were randomized. Additionally, pairs of pooled reference samples were inserted in the queue at intervals of approximately one per every 20 samples for quality control and data standardization. Samples were prepared for each method using extraction procedures that were matched for use with the chromatography conditions. Data were acquired using LC-MS systems comprised of Nexera X2 U-HPLC systems (Shimadzu Scientific Instruments) coupled to Q Exactive/Exactive Plus Orbitrap mass spectrometers (ThermoFisher). The method details are summarized below.

Article



LC-MS Method 1: HILIC-pos (positive ion mode MS analyses of polar metabolites)

LC–MS samples were prepared from plasma samples by protein precipitation with the addition of nine volumes of 74.9:24.9:0.2 v/v/v acetonitrile/methanol/formic acid containing stable isotope-labelled internal standards (valine-d8, Isotec; and phenylalanine-d8, Cambridge Isotope Laboratories). The samples were centrifuged (10 min, 9,000g, 4 °C), and the supernatants injected directly onto a 150 \times 2-mm Atlantis HILIC column (Waters). The column was eluted isocratically at a flow rate of 250 μ l/min with 5% mobile phase A (10 mM ammonium formate and 0.1% formic acid in water) for 1 min followed by a linear gradient to 40% mobile phase B (acetonitrile with 0.1% formic acid) over 10 min. MS analyses were carried out using electrospray ionization in the positive ion mode using full scan analysis over m/z 70–800 at 70,000 resolution and 3-Hz data acquisition rate. Additional MS settings were: ion spray voltage, 3.5 kV; capillary temperature, 350 °C; probe heater temperature, 300 °C; sheath gas, 40; auxiliary gas, 15; and S-lens RF level 40.

LC-MS Method 2: HILIC-neg (negative ion mode MS analysis of polar metabolites)

Samples (30 μ l) were precipitated by the addition of four volumes of 80% methanol containing inosine-15N4, thymine-d4 and glycocholate-d4 internal standards (Cambridge Isotope Laboratories). The samples were centrifuged (10 min, 9,000g, 4 °C), and the supernatants were injected into a 150 \times 2.0-mm Luna NH2 column (Phenomenex). The column was eluted at a flow rate of 400 μ l/min with initial conditions of 10% mobile phase A (20 mM ammonium acetate and 20 mM ammonium hydroxide in water) and 90% mobile phase B (10 mM ammonium hydroxide in 75:25 v/v acetonitrile/methanol) followed by a 10-min linear gradient to 100% mobile phase A. MS analyses were carried out using electrospray ionization in the negative ion mode using full scan analysis over m/z 60–750 at 70,000 resolution and 3 Hz data acquisition rate. Additional MS settings were: ion spray voltage, –3.0 kV; capillary temperature, 350 °C; probe heater temperature, 325 °C; sheath gas, 55; auxiliary gas, 10; and S-lens RF level 40.

LC-MS Method 3: C18-neg (negative ion mode analysis of metabolites of intermediate polarity; for example, bile acids and free fatty acids)

Samples (30 μ l) were extracted using 90 μ l methanol containing PGE2-d4 as an internal standard (Cayman Chemical Co.) and centrifuged (10 min, 9,000g, 4 °C). The supernatants (10 μ l) were injected onto a 150 \times 2.1-mm ACQUITY BEH C18 column (Waters). The column was eluted isocratically at a flow rate of 450 μ l/min with 20% mobile phase A (0.01% formic acid in water) for 3 min followed by a linear gradient to 100% mobile phase B (0.01% acetic acid in acetonitrile) over 12 min. MS analyses were carried out using electrospray ionization in the negative ion mode using full scan analysis over m/z 70–850 at 70,000 resolution and 3 Hz data acquisition rate. Additional MS settings were: ion spray voltage, –3.5 kV; capillary temperature, 320 °C; probe heater temperature, 300 °C; sheath gas, 45; auxiliary gas, 10; and S-lens RF level 60.

LC-MS Method 4: C8-pos

Polar and nonpolar lipids were extracted from 10 μ l samples using 190 μ l isopropanol containing 1-dodecanoyl-2-tridecanoyl-snglycero-3-phosphocholine as an internal standard (Avanti Polar Lipids; Alabaster, AL). After centrifugation (10 min, 9,000g, ambient temperature), supernatants (10 μ l) were injected directly onto a 100 \times 2.1-mm ACQUITY BEH C8 column (1.7 μ m; Waters). The column was eluted at a flow rate of 450 μ l/min isocratically for 1 min at 80% mobile phase A (95:5:0.1 v/v/vl 10 mM ammonium acetate/methanol/acetic acid), followed by a linear gradient to 80% mobile phase B (99.9:0.1 v/v methanol/acetic acid) over 2 min, a linear gradient to 100% mobile phase B over 7 min, and then 3 min at 100% mobile phase B. MS analyses were carried out using electrospray ionization in the positive ion mode using full scan analysis over m/z 200–1,100 at 70,000 resolution and 3 Hz data acquisition rate. Additional MS settings were: ion spray voltage, 3.0 kV; capillary temperature, 300 °C; probe heater temperature, 300 °C; sheath gas, 50; auxiliary gas, 15; and S-lens RF level 60.

Metabolomics data processing

Raw LC-MS data were acquired to the data acquisition computer interfaced to each LC-MS system and stored on a robust and redundant file storage system (Isilon Systems) accessed via the internal network at the Broad Institute. Non-targeted data were processed using Progenesis QIsoftware (v 2.0, Nonlinear Dynamics) to detect and de-isotope peaks, perform chromatographic retention time alignment, and integrate peak areas. Additionally, chromatograms were automatically integrated and visually inspected for an acceptable integration using TraceFinder 3.3 (or later versions; ThermoFisher) for specific metabolites of known identity. Temporal drift was monitored and normalized with the intensities of peaks measured in the pooled reference samples.

Cell culture

HepG2 cells (ATCC, #HB-8065) were maintained in Dulbecco's Modified Eagle Medium (DMEM) containing 10% fetal bovine serum (FBS) and 1% penicillin-streptomycin (PS) in a 5% $\rm CO_2$ environment at 37 °C in a humidified incubator. For insulin-signaling experiments, cells on 12-wells plate were starved for 16h (in DMEM+0.1% BSA) and then stimulated with 100 nM insulin for 15 min. Six hours before insulin stimulation, itaconate (#I29204, Sigma), mesaconate (#131040, Sigma), or citraconate (#C82604, Sigma) were added into the wells to give final concentrations of 1 or 10 μ M, a concentration well within the physiological range. Cells were washed with PBS 1X and harvested with RIPA lysis buffer (#20-188, Millipore) containing protease and phosphatase inhibitors (#B14002, #B15002, BioTool). For the time-course experiments, cells were grown on 24-well plates and treated with itaconate, mesaconate, or citraconate at 10 μ M concentration, then returned to the incubator and harvested 3, 6, and 24h after metabolite addition. Cells without treatment were considered the 0h time-point. In all cases, at the indicated time, the cells were washed with PBS 1X and collected with Trizol (#15-596-018, Life Technologies). The RNA was extracted as described above, and the samples were submitted to real-time qPCR analysis.





In some experiments, to access the transcription-dependent effects of itaconate, mesaconate, and citraconate, the HepG2 cells were treated with the transcription inhibitor triptolide (100 nM, 2h, #HY-32735, MedChemExpress), then subjected to 6h of metabolite (10 µM) treatment, after which the cells were washed and the RNA collected for real-time qPCR analysis.

For the luciferase assays, HepG2 on 96-well plates were transfected with plasmids containing the PGC1α proximal promoter (#154259, Addgene), PPAR response elements (#1015, Addgene), SREBF1 response elements (#90371, Addgene), and LXR response elements (#90348, Addgene) using Lipofectamine 3000 (#L3000015, ThermoFisher). 48 hours after transfection, the cells were lysed and luciferase activity was analyzed using the Dual-Glo Luciferase assay system (#E2940, Promega). Bioluminescence was read using a plate reader CLARIOstar (BMG LABTECH), and the data was normalized by Renilla values.

In some experiments, PPAR α knockdown was performed. To this end, HepG2 cells were transfected with PPAR α siRNA (5 pmol/well, #J-003434-05-0002, Horizon Discovery) using Lipofectamine RNAiMAX (#13778150, ThermoFisher). 48h after the transfection, cells were treated with the metabolites at a concentration of 10 μ M for 6h, and RNA extracted for gene expression analysis by qPCR. Alternatively, to activate PPAR α , cells were treated with the PPAR α antagonist, GW6471 (#HY-15372, MedChemExpress) at 10 μ M for 24h before collection.

To assess lipogenesis, HepG2 cells were starved for 16h (DMEM+0.1% BSA) and treated with [14 C] acetate (0.3 μ Ci/well) for 6h in the absence or presence of insulin (100 nM) and itaconate, mesaconate, or citraconate at 10 μ M. Lipids were extracted from the cells using hexane:isopropanol (3:2), resuspended in toluene, and the radioactive acetate incorporation determined by scintillation counting.

Immunoblotting analysis

Cells lysates were collected in RIPA lysis buffer containing protease and phosphatase inhibitors, homogenized and protein concentration assessed using Bicinchoninic Acid Protein Assay. Then equal protein amounts (8-12 μ g) were submitted to SDS-PAGE, transferred to a nitrocellulose membrane, and the membranes incubated with primary antibodies for Phospho-IGF-I Receptor β (Tyr1150/1151) (#3024, Cell Signaling), Insulin Receptor β (#3025, Cell Signaling), Phospho-Akt (Ser473) (#4060, Cell Signaling), Akt (#4685, Cell Signaling), SREBP-1 (#SC-8984, Santa Cruz), FAS (#ab22759, ABCAM), ACC (#3662, Cell Signaling), PPAR α (#ab8934, ABCAM), ACSL1 (#9189, Cell Signaling), or β -actin (#SC8432-HRP, Santa Cruz). Membranes were washed and incubated with appropriate secondary antibodies followed by incubation with chemiluminescent reagent SuperSignal West Pico PLUS (#34580, ThermoFisher).

Assessment of Mitochondrial Function

For mitochondrial experiments, AML12 hepatocytes (ATCC, #CRL-2254) were cultured in DMEM (10% FBS, 1% PS, 10 μ g/mL insulin, 5.5 μ g/mL transferrin, 5 ng/mL selenium, 40 ng/mL) and plated into 96-well, treated for 6h with itaconate, mesaconate or citraconate (10 μ M). For the mitochondrial stress test, the media was changed to running media (Seahorse XF DMEM medium, 10 mM glucose, 1 mM sodium pyruvate, 2 mM glutamine), and the cells were incubated for 1 h at 37°C without CO₂. The plate was transferred to the XFe96 Seahorse Extracellular Flux Analyzer (Seahorse Bioscience, MA, USA) for pneumatic injection of oligomycin (2 μ M final concentration), carbonyl cyanide-4-(trifluoromethoxy)phenylhydrazone (FCCP, 1 μ M), and rotenone (0.1 μ M)/antimycin A (2.5 μ M), and measurement of oxygen consumption rate (OCR). On the same plate, some of the cells were treated for 2h with 100 nM triptolide (#HY-32735, MedChemExpress) to inhibit transcription before the metabolite addition. Another parallel group of cells were treated with the mitochondrial pyruvate carrier (MPC) inhibitor, UK5099 (2 μ M, #4186, Tocris), to analyze pyruvate uptake dependency.

For the glycolysis stress test, AML12 cells were seeded on 96-well plates, the media was changed to running media (Seahorse XF DMEM medium, 2 mM glutamine, but without glucose or pyruvate) and extracellular acidification rate (ECAR) was measured in response to glucose (10 mM final concentration), oligomycin (2 μ M final concentration), 2-Deoxy-D-glucose (50 mM final concentration). For the mitochondrial membrane potential experiment, HepG2 cells were treated for 6h with the metabolites as described above (10 μ M), detached with 0.25% trypsin-EDTA solution for 5 minutes, washed with PBS 1X, and exposed to the MitoTracker Red FM dye (#M22425, ThermoFisher) for 30 min. The cells were then washed, resuspended in PBS 1X, filtered through a 100 μ M mash and submitted to FACS analysis using a Beckton Dickenson FACSAria (BDBiosciences).

In vivo treatment with itaconate and mesaconate

Male C57Bl/6J (B6J) at 8-week-old on chow diet were injected intraperitoneally with saline, itaconate (#I29204, Sigma), or mesaconate (#I31040, Sigma) for 3 consecutive days at 10 mg/Kg. Six hours after the last injection, the mice were sacrificed, and liver tissue was collected for gene expression or mitochondrial function. For the latter, approximately 50 mg of liver was homogenized in mitochondrial respiration medium (MIR) using a Dounce homogenizer. Samples (20 mg) were added to an Oxygraph-2k sample chamber (Oroboros Instruments, Innsbruck, Austria) and maintained at 37°C. Malate (0.5 mM) and glutamate (10 mM) were injected first, followed by ADP (2.5 mM) for Complex I-dependent O_2 consumption. Coupling capacity was measured by adding oligomycin (2.5 mM) and uncoupling capacity measured after addition of 1 mM FCCP (carbonyl cyanide p-trifluoromethoxyphenylhydrazone). After stabilization, the Complex I inhibitor rotenone (1 mM) and the Complex III inhibitor antimycin A (5 mM) were added to determine Complex II-mediated respiration.

Article



Primary Hepatocytes Isolation

For primary hepatocytes isolation, chow or HFD-fed mice were anesthetized, following by liver perfusion with Krebs-Ringer buffer (containing 100 μ M EGTA) and DMEM (10% FBS, 1% PS, 1.2 mg/mL type I collagenase). The liver was disrupted to release the cells, filtered through a 100 μ m strainer, and centrifuged at 50 g for 3 min, at 4°C. The hepatocyte's pellet was resuspended in 10 mL DMEM (10% FBS, 1% PS), and 10 mL of Percoll solution (90% in PBS) was added, followed by centrifugation at 700x g for 5 min, at 4°C. The cells were washed with cold PBS, counted and plated in pre-coated plates with collagen I (Sigma, #C8919). Four hours after plating, cells were gently washed to remove floating cells, and fresh DMEM (10% FBS, 1% PS) was added. For insulin-signaling experiments, the hepatocytes on 12-wells plate were serum starved for 16h (in DMEM+0.1% BSA) followed by insulin stimulation (100 nM, 15 min). Six hours before insulin stimulation, itaconate (#I29204, Sigma), mesaconate (#131040, Sigma), or citraconate (#C82604, Sigma) were added into the wells (10 μ M). Finally, cells were washed with PBS 1X and collected with RIPA lysis buffer (#20-188, Millipore) with protease and phosphatase inhibitors (#B14002, #B15002, BioTool). For lipid staining with BODIPY (#D3823, Invitrogen), primary hepatocytes were cultured in DMEM (10% FBS, 1% PS) and metabolites were added into the wells (10 μ M) for 6 hours. Two wells/ group were assigned for imaging, and 10 wells/group for cell lysing and fluorescence measurement. For qPCR, primary hepatocytes in complete media (DMEM+10% FBS+1% PS) were treated with metabolites for 6h, at 10 μ M. The cells were washed with PBS 1X and collected with Trizol (#15-596-018, Life Technologies). The RNA was extracted as described before, and submitted to real-time qPCR analysis.

QUANTIFICATION AND STATISTICAL ANALYSIS

Following the processing of the metabolomics data and the identification of metabolites, the dataset was subjected to analysis utilizing weights and mean-variance trends within the linear modeling framework provided by the limma package. ^{67,68} Tests were adjusted for multiple testing using the Benjamini-Hochberg false discovery rate (FDR). Metabolites enrichment in the portal or cardiac blood were defined by fold change >1.25 and p-value<0.05 by paired comparison of the metabolite abundance in the portal blood compared to cardiac blood. Unpaired comparison was performed to identify metabolites changed by treatment (i.e. HFD, Vancomycin, and Metronidazole). Pearson's correlations were performed to access interaction of specific bacteria strains or metabolites with metabolic parameters. For physiological and experimental data one-way ANOVA followed by Tukey's post-test was performed. Data were represented as mean ± standard error of the mean (SEM).